Antioxidants and Redox Signaling

DOI: 10.1089/ars.2018.7615

Original Research Communication

Quantitative analyses of the yeast oxidative protein folding pathway *in vitro* and *in vivo*

Dave M Beal, Emma L Bastow, Gemma L Staniforth, Tobias von der Haar, Robert B Freedman[1*] and Mick F Tuite

Kent Fungal Group, School of Biosciences

University of Kent

Canterbury, Kent CT2 7NJ, UK

[1]School of Life Sciences, Gibbet Hill Campus, University of Warwick, Coventry, CV4 7AL.

*Deceased

Words = 3903, References = 67

Running head: Yeast oxidative protein folding pathway

Key words: disulfide bond/endoplasmic reticulum/protein disulfide isomerase/ERO1

Abstract

Aims: Efficient oxidative protein folding (OPF) in the endoplasmic reticulum (ER) is a key requirement of the eukaryotic secretory pathway. In particular, protein folding linked to the formation of disulfide bonds, an activity dependent on the enzyme protein disulfide isomerase (PDI), is crucial. For the *de novo* formation of disulphide bonds, reduced PDI must be re-oxidised by an ER-located oxidase (ERO1). Despite some knowledge of this pathway, the kinetic parameters with which these components act and the importance of specific parameters, such as PDI reoxidation by Ero1, for the overall performance of OPF *in vivo* remain poorly understood.

Results: We established an *in vitro* system using purified yeast (*Saccharomyces cerevisiae*) PDI (Pdi1p) and ERO1 (Ero1p) to investigate OPF. This necessitated the development of a novel reduction/oxidation processing strategy to generate homogenously oxidised recombinant yeast Ero1p. This new methodology enabled the quantitative assessment of the interaction of Pdi1p and Ero1p *in vitro* by measuring oxygen consumption and reoxidation of reduced RNAase A. The resulting quantitative data were then used to generate a simple model which can describe the oxidising capacity of Pdi1p and Ero1p *in vitro* and predict the *in vivo* effect of modulation of the levels of these proteins.

Innovation: We describe a model that can be used to explore the OPF pathway and its control in a quantitative way.

Conclusion: Our study informs and provides new insights into how OPF works at a molecular level and provides a platform for the design of more efficient heterologous protein expression systems in yeast.

Introduction

The oxidative protein folding (OPF) pathway of the endoplasmic reticulum has been well-characterized in the yeast *Saccharomyces cerevisiae*, both in terms of identification of components and defining how they interact. The key components of the pathway are protein disulfide isomerase (Pdi1p) (13) and endoplasmic reticulum oxidase (Ero1p) (16, 41), encoded by the essential *PDI1* and *ERO1* genes respectively. Biochemical, structural and genetic characterization of the pathway has demonstrated that it comprises a linear electron transfer pathway. Electrons from the thiol (SH) groups of reduced proteins flow via Pdi1p to Ero1p through a series of thiol:disulfide oxidoreductions, to a bound FAD group within Ero1p, and thence to molecular oxygen. The net result of this process is the formation of disulfide (S-S) bonded proteins and hydrogen peroxide (18, 19, 55, 56).

Given the similarities in the core components of the yeast and human OPF systems, it is not surprising that some functional complementation of components between the species has been observed both *in vivo* (38) and *in vitro* (4). Despite this, there are marked differences between species in the number of members of the PDI and ERO families, in their regulation, and in the associated components of the pathway. Yeast and human ERO proteins show functional identity but also significant structural differences, especially in the number and arrangement of non-active-site disulfide bonds (18, 25). These disulfides play regulatory roles which differ considerably between the species, although both in yeast and human systems, the formation and breakage of regulatory disulfides in ERO is critically catalysed by PDI (1–3, 5, 7, 8, 28, 43). Recently it has been proposed that the mode of regulation of oxidative protein folding differs between humans and yeast in that the human pathway provides for clear on/off switching whereas regulation in the yeast system is more graduated (37, 66).

In *S. cerevisiae*, a simple linear pathway operates and both *ERO1* and *PDI1* are essential genes. However, viability of the *pdi1* deletion strain can be restored by overexpression of a number of alternative PDI-like genes such as *EUG1* (52). In contrast, human cells lacking both ERO genes (α and β) are viable in part because other proteins are available in the ER that can function as electron acceptors from PDI. These include the peroxidases GPX7 and

8 and possibly the peroxiredoxin PrxIV, which can use H_2O_2 generated by ERO or other systems, as terminal electron acceptor (26, 36, 42, 53, 59, 67). Such activities are lacking in the yeast ER. Furthermore, the human pathway is also more complex in that a large number of PDI family members can interact with ERO in either a regulatory or catalytic electron transfer role (34, 50).

In order to better understand the OPF pathway and its regulation, PDI-dependent electron transfer has been effectively reconstituted *in vitro* using purified proteins where pathway activity can be assayed by monitoring formation of disulfide-bonded proteins (30, 54) or consumption of O_2 (57, 58)(**Figure 1**) (27).

Disulfide-bonded proteins including antibodies, cytokines and serum proteins are valuable biopharmaceuticals and *S. cerevisiae* remains an attractive, safe and low cost host cell in which to generate them (47, 65). Many of these high value biopharmaceuticals contain inter- and/or intramolecular disulfide bonds and thus need to transit through the ER in order to be correctly folded. However, the secretory capacity of *S. cerevisiae* is low and has to deal with many fewer secreted proteins than a mammalian cell, for example. As a result, there have been attempts to engineer OPF to increase the production of such high-value, disulfide-bonded targets. Indeed, overexpression of yeast and human PDI in yeast was shown at an early stage to improve the production of a range of recombinant disulfide-bonded proteins (44, 47) and this strategy is exploited industrially in the production of human serum albumin and transferrin, for example (14, 40).

While showing a degree of success in terms of improving product yield and/or authenticity, interventions intended to increase the yield of the pathway in production and secretion of recombinant proteins can have unexpected outcomes (see e.g. ref (45)). A key issue is that knowledge of kinetic properties of the components and quantitative analyses of the pathway are lacking and this deficit has discouraged systems biology approaches to rational engineering of the OPF pathway (57). In this work, we have reconstituted the OPF of *S. cerevisiae in vitro* and obtained the first quantitative data on the kinetics of the overall system and developed a model capable of predicting how the system can be modified to enhance oxidative protein folding. Such information will underpin future

design strategies for enhanced secretion of high value complex biopharmaceuticals from this simple eukaryote.

Results

Production of active recombinant Pdi1p and Ero1p

To date biochemical studies using Pdi1p have relied on bacterially produced protein, which is biochemically active (29, 30, 37, 57). In native environments, a 21 residue N-terminal signal sequence directs Pdi1p to the ER where it is then cleaved to give the mature and functional protein. To mimic functional Pdi1p and increase protein yield in bacterial expression systems it is common to remove the signal sequence from the construct and replace it with a poly histidine tag (30, 54, 57). We used this strategy to obtain highly pure $Pdi1p_{22\text{-}530}$, lacking the signal sequence but containing an N-terminal six histidine tag (**Figure 2A**).

In contrast to Pdi1p, Ero1p does not express well as a full-length construct and consequently, previous studies have relied on truncated Ero1p constructs (10, 18). We chose to use the longest Ero1p construct we could express in reasonable yield in *E. coli* without mutation of Cys residues ($Ero1p_{19\text{-}424}$), again with an N-terminal six histidine tag to facilitate purification. The resulting purified $Ero1p_{19\text{-}424}$ existed as a mixture of oxidation products post-purification. To yield homogeneously oxidised $Ero1p_{19\text{-}424}$ containing stoichiometric amounts of FAD we exploited a controlled sequence of reduction and oxidation in the presence of FAD (**Figure 2B**). Using an assay for oxygen consumption in a DTT-dependent manner (**Figure 2C**), we were able to demonstrate that the $Ero1p_{19\text{-}424}$ reproducibly consumed oxygen with general kinetic characteristics as reported by others (37, 57) (**Figure 2D**). Our homogeneously oxidised $Ero1p_{19\text{-}424}$ had a maximum rate of 0.8 µM O_2 per µM Ero1p per second when treated with 10 mM DTT.

Rate of thiol oxidation is linearly dependent on Pdi1p and Ero1p concentrations

GSH-mediated oxygen consumption (**Figure 1**, Assay 1) was used to study the limits of the coupled system using variable Ero1p and Pdi1p concentrations. At a fixed 1 µM concentration of Ero1p, the rate of oxygen consumption was dependent on the

concentration of Pdi1p (**Figure 3 A, B**). This dependence was linear at concentrations below 15 µM before the system saturated (**Figure 3C**). Conversely, at a fixed 5 µM concentration of Pdi1p, the maximum rate was linearly dependent on Ero1p at concentrations up to 2 µM (**Figure 3D**). In both cases, the maximum rate of oxygen consumption observed in saturating conditions was approximately 1.5 µM s^{-1}.

Although GSH is present within the ER the physiological substrates of Pdi1p are proteins. A frequently used model substrate *in vitro* is reduced and denatured Ribonuclease A (30, 54), a single chain protein containing 4 intra-chain disulfide bonds. In the GSH-dependent assay of the Pdi1p/Ero1p interaction, the electron donor, GSH, is present in vast excess. When GSH is replaced as an electron source by reduced and denatured RNase A (rdRNase A) the number of electrons available to the system is limited by the solubility of the rdRNase A. Using the rdRNase A assay (**Figure 1**, Assay 2), we found that at 60 µM rdRNase A (i.e. 240 µM disulfides) and 1 µM Ero1p, the maximum rate of oxygen consumption was again linearly dependent on the concentration of Pdi1p, reaching saturation above 10 µM (**Figure 4A, B**). Similarly, at 5 µM Pdi1p the rate was dependent on Ero1p concentrations (**Figure 4B**). Oxygen consumption correlated with a change in redox state of the RNase A (**Figures 4C, S1**), and the observed formation of disulfide bonds in the protein was clearly dependent on the presence of both Pdi1p and Ero1p (**Figure 4D**). It is noteworthy that at a substrate:Pdi1p:Ero1p ratio of 60:5:1 the substrate can be fully reoxidised within 20 min in this assay.

The pH dependence of the Pdi1p/Ero1p catalytic cycle

To determine the optimum pH of the GSH-promoted Pdi1p and Ero1p catalytic cycle the interaction of 5 µM Pdi1p and 1 µM Ero1p was assessed at different pH values (**Figure 5A, B**). This analysis showed an extreme dependence on the pH of the reaction for the GSH-driven system with a narrow window of optimum activity focussed around pH8. In contrast to this narrow activity range observed with GSH as the electron source, the system driven by 60 µM RNAse A showed broader tolerance to fluctuations in pH (**Figure 5B**). We were unable to find reported values for the pH of the yeast ER, although for mammalian cells

this has been reported as 7.5 (33, 39). Thus, under these pH conditions, proteins would be the preferred substrate for Pdi1p despite the presence of GSH.

The relation between Pdi1p oxidation state and refolding activity

To examine in more detail how the internal oxidation state of Pdi1p relates to oxidative refolding activity in our *in vitro* system, a PEG-trapping assay was exploited which, through alkylation of reduced cysteines, leads to defined shifts in apparent molecular weight (48). Analysis of PEG-treated Pdi1p over the course of the oxidative refolding reaction by western blotting showed that within 100 sec of RNase A refolding, the initially fully oxidised Pdi1p becomes heavily reduced with a prominent species appearing at a size expected for four reduced cysteines, as well as a less abundant species corresponding to six reduced cysteines i.e. fully reduced Pdi1p (**Figures 6A, B and S2, S3**).

Niu *et al*. (37) predicted that a fully reduced species of Pdi1p should form under strongly reducing conditions, which is the case for our *in vitro* system (**Figure 6 A, B, and S2, S3**). This suggests that our assays operate in the high Ero1p activity regime proposed by Niu *et al*., (37). However, contrary to these data, we observed that the maximal activity of 5 µM Pdi1p and 1µM Ero1p occurred between 400 and 600 sec, when these more reduced components would have been depleted from the mixture (**Figure 6 A and S2**). The presence of these more reduced forms of Pdi1p at the very beginning of the reaction rather than during the more active period of activity, implies that reduction is a side effect of Ero1p activation rather than controlling the rate of Pdi1p activity.

Our data also showed that different ratios of Pdi1p to Ero1p consume oxygen, and therefore reoxidise RNase A, at different rates (**Figure 4A, B**). Comparison of the redox poise of the Pdi1p, the distribution of oxidation states, over the course of these reactions (**Figure 6A, B and S2, S3**) showed that at 5:1 Pdi1p:Ero1p ratio, Pdi1p returns to a basal state of oxidation, consisting of fully oxidised Pdi1p but with a significant proportion with 1 reduced disulfide, much faster than an equimolar (1:1) ratio (**Figure 6C**).

Modelling oxidative folding

Our biochemical assays interrogate oxidative protein folding from several different angles. We sought to unify the quantitative information from these assays by using an ODE-based mathematical model of the biochemical reactions. In establishing the model, we made several design decisions. For example, previous studies have shown that Pdi1p has asymmetric active sites with only one of the CGHC motifs responsible for the oxidase activity and the other being more important for isomerase activity (30). Consequently, to simplify modelling, we only utilised one Pdi1p active site in our model. Several reactions, such as the oxidation of Ero1p by molecular oxygen, are in reality multi-step reactions. However, these are likely fast reactions, and as a consequence we modelled these as a single-step reaction. The reduction of oxidised Pdi1p by GSH likely occurs by sequential reaction with two consecutive GSH moieties, which are biochemically very similar. Because of their similarity we assumed that these reactions occur with identical rates. However, as we show below, the rate constants for these reactions are not limiting for the time evolution of the model so this has no consequences for deriving the remaining, limiting rate constants. In initial model runs we also experimented with the inclusion of an inhibiting reaction between peroxide and Pdi1p, but since this did not alter the behaviour of the model, we did not include this reaction in our final runs. We did however include an initial activation step involving the sequential reduction of two regulatory disulfides which yields active Ero1p. This step was introduced to account for the clear presence of a lag phase in our biochemical assays (**Figure 3A**), but also to reflect the published biochemical evidence for such a step (37, 49).

Based on these considerations, the structure of the final model was assembled (**Figure 7A)** and implemented in the COPASI biochemical simulator (21). Following initiation of the model with the known input concentrations of the molecular components, we then sought to determine the reaction rates by parameter fitting to our experimentally determined oxygen consumption in the system.

We initially observed that the model found well-fitting solutions with very different parameter combinations, indicating that the model was strongly underdetermined. We

therefore experimentally determined rates for Ero1p oxidation, by observing oxygen consumption in reactions containing only Ero1p and varying concentrations of DTT (**Figure S6**). In addition, we characterised the diffusion of environmental oxygen into the Clarke cell by depleting oxygen with sodium dithionite, and by determining rates of recovery of the oxygen concentration in the open cell (**Figure S4**). When we fixed the rates for these reactions using the experimentally determined values and repeated the parameter fitting exercise, all rate constants except the Pdi1p:GSH interaction were reproducibly determined within very narrow ranges (**Figure 7B and S5**). When compared to the experimental oxygen consumption data (o), the predicted oxygen consumption curves (x) at different Pdi1p and Ero1p concentrations showed excellent correlation (**Figure 7C**), with a non-linear increase in maximum $\delta[O_2]/\delta t$ when the Pdi1p concentration is increased above 15:1 Pdi1p:Ero1p (**Figure 7D**).

In vitro rates and their relation to OPF activity in vivo

The measuring of biochemical activity *in vitro*, and the interpretation of this activity *in silico*, provides quantitative information that can be used to explore characteristics of the OPF pathway *in vivo*. Intracellular levels of Pdi1p and Ero1p in yeast have been reported as 28,000 and 5,200 molecules per cell, respectively, in recent high-quality proteome datasets (22). Given estimated ER volumes of 0.2-0.4 um^3 (62), this would be equivalent to concentrations of 155 and 29 µM. To estimate the substrate flux processed by these factors, we identified from recent proteomics studies (15, 23, 51, 60, 63) all proteins residing in or passing through the ER (i.e. all proteins reported to be present in the ER, Golgi, endosome, vacuole, cell wall, or reported to be extracellular). We combined these data with published protein turnover rates (9) and with the number of cysteines per protein, to arrive at an estimate of around 269,000 cystines formed per minute. This assumes that every single cysteine pair present in all proteins passing through the ER is converted to a cystine through Pdi1p activity, which is unlikely to be the case. This value is thus an upper limit only, and likely substantially overestimates the need for catalysed disulfide bond formation.

In our *in vitro* experiments, the maximal capacity of Pdi1p for disulfide bond formation (i.e. when both Ero1p and glutathione are provided in excess) is approximately 15 disulfide bonds per minute per Pdi1p molecule (estimated from the data in **Figure 3D**). Thus, if sufficient Ero1p is present *in vivo*, the estimated Pdi1p population in yeast could process up to 400,000 disulfide bonds per minute. The *in vivo* Ero1:Pdi1 ratio of roughly 1 in 5 is slightly below the ratio where Ero1p becomes saturating *in vitro* (2:5, **Figure 3D**), indicating that *in vivo* Pdi1p activity might be limited by Ero1p availability. On the other hand, Pdi1p can also act as an isomerase in addition to forming disulfide bonds, in reactions that are net neutral in terms of electron flow but that nevertheless remove Pdi1p molecules from the active pool while the isomerisation reactions are being catalysed. This would reduce the effective Pdi1p concentration itself.

In order to analyse how well these estimates reflect the biology of yeast cells, we tested experimentally how such cells cope with an enforced reduction of their Pdi1p content, using strains in which the original promoter was replaced by a Tet-responsive tetO7promoter that is repressible by addition of doxycycline to the growth medium (6). We observed that substantial Pdi1p depletion can be tolerated with only a minor reduction in growth rates. At the highest doxycycline concentration used in our experiment, Pdi1p concentrations were reduced to 23 % of the wild type content (**Figure 8A and S9A**), yet this still permitted growth at 24 % of the wild type growth rate. Moreover, the ratio of observable Pdi1p oxidation states was not substantially affected by this depletion either **(Figure 8B or S9B)**. In contrast to the monotonic decrease of both Pdi1 content and growth rates with doxycycline concentration in a Tet-*PDI1* strain, Ero1p levels showed a more complex relationship between the corresponding parameters (**Figure 8B and S9C**). In the absence of doxycycline the promoter replacement strain contained higher levels of Ero1p than the control. Interestingly however, this increased expression coincided with a reduction in growth rates of 5-10%. Upon addition of doxycycline at increasing concentrations, Ero1p levels initially dropped but then recovered slightly around the 0.4 mg/l mark. Growth rates moved parallel to the Ero1p content, initially dropping before recovering and then dropping again (cf the inset panel in **Figure 8B**). Interestingly, in our blot the Ero1p band displayed as an apparent double band, and

the depletion of Ero1p in the doxycycline-repressible strain coincided with a clear shift from a predominantly lower molecular weight isoform to a higher molecular weight one and low Ero1p levels. We interpret this overall complex behaviour as evidence for some currently not understood regulation of Ero1p expression, possibly involving post-translational modifications which may be regulated by feedback loops (since it is dependent on intracellular Ero1p levels).

Notably though, like the Tet-*PDI1* strain the Tet-*ERO1* strain allows substantial growth to occur even when this protein is depleted to less than 25% of wild type levels. These observations corroborate our *in silico* prediction that the oxidative capacity in *S. cerevisiae in vivo* comfortably exceeds the required capacity.

Discussion

S. cerevisiae is a well-exploited host system for the production of secreted recombinant proteins due in part to its potential to carry out post-translational modifications such as inter- and intra-molecular disulfide bond formation. However, the secretory capacity of *S. cerevisiae* cells is far less than that of cultured mammalian cells, presumably as a consequence of a less developed OPF pathway that has not evolved to handle the secretion of large amounts of secretory proteins. Yet this yeast species has been successfully engineered to yield commercially viable levels, but this has been done empirically rather than in a directed and informed manner. The latter requires a systematic understanding of the yeast OPF pathway and its regulation using both *in vivo* and *in vitro* approaches, with the latter being hampered by inefficient methods for isolating key OPF components, in particular the ER-located oxidase Ero1p (57).

In this study we have developed an efficient reduction/oxidation processing strategy to generate homogenously oxidised yeast Ero1p expressed in *E. coli* strains. This new methodology has for the first time enabled the *in vitro* quantitative assessment of the interaction of Pdi1p and Ero1p by measuring oxygen consumption and GSSG formation through NADPH-coupled assays. The resulting quantitative data have allowed us to generate a simple model which can describe the oxidising capacity of Pdi1p and Ero1p *in vitro* and predict the *in vivo* effect of modulation of the levels of the key components of

the OPF, thereby allowing us to begin to explore yeast oxidative folding in a quantitative way. Overall, our study informs and provides new insights into how oxidative protein folding works at a molecular level.

One fundamental difference between yeast and mammalian PDI and ERO1 proteins is that the yeast proteins are glycosylated *in vivo* while here we carry out *in vitro* studies exclusively with non-glycosylated proteins produced in *E. coli*. The report that the specific activities of the natural glycosylated yeast Pdi1p versus a recombinant, non-glycosylated form are similar (31) would suggest that the presence or absence of N-glycans has little or no effect on the isomerase activity of this enzyme although detailed equivalent comparisons for Ero1p have not to our knowledge been reported in the literature.

Overall, our study informs and provides new insights into how oxidative protein folding works at a molecular level. The yeast ER is more strongly oxidising than the cytoplasm, with a GSH:GSSG ratio of 1:1 to 3:1 in the ER compared with 30:1 to 100:1 in the cytoplasm (24), meaning that GSH concentrations may reach 10 mM based on measured total glutathione concentrations in the ER of HeLa cells (35). If GSH is readily available as an electron source for the oxidative folding machinery, it is not clear how proteins could compete for access to Pdi1p. Our observations of the extreme pH dependence of Pdi1p oxidation by GSH, but not by a protein substrate (**Figure 5**), suggests that this interference is not relevant at the reported pH within the ER (12). The potential for continuous, futile cycles of GSH-mediated reduction and oxidation was proposed as a significant issue (57) to the "active site asymmetry" model of Pdi1p activity proposed by Kulp *et al* (30). The observation of the strong pH-dependence of such futile cycles therefore adds weight to this model. Interestingly, pH dependence has also been observed for the human PDI/ERO interaction (4). Assessment of the oxidation of rdRNAse A in the absence of either Pdi1p or Ero1p, at pH 8 where spontaneous oxidation would be faster than in the ER where the pH is 7.5, shows that non-enzyme mediated substrate oxidation is far slower than that observed in the catalysed processes **(Figure S7)** and therefore are not able to account for difference in activity between the two electron sources.

Another observation that is consistent with the "active site asymmetry" model, which posits that one active site is utilised as an oxidase and the other as a reductase and an isomerase, is our inability to observe completely oxidised Pdi1p, either *in vitro* or *in vivo*. At the end of the *in vitro* experiment, when reduced RNase A is consumed, the resting state of the Pdi1p contains a significant proportion of Pdi1p containing a single reduced disulfide (**Figure 6A, B and S2, S3**). Similarly, even when Pdi1p levels are significantly reduced *in vivo*, the proportion of reduced to oxidised protein are not altered (**Figure 8A** and **S9B**).

Comparison of the modelled system to the *in vivo* environment of the yeast ER suggests that the total oxidation capacity of a yeast cell is 400,000 disulfide bonds per minute, not considering alternative roles of Pdi1p such as isomerisation, which would diminish this capacity. *In silico* assessment of the secretory pathway, which OPF is part of, suggests a maximum requirement of 269,000 disulfides to be formed per minute. This is likely a substantial over estimate of the real required rate, since few proteins contain all their cysteines within Pdi1p-catalysed disulfide bonds. Depletion experiments confirm the notion that Pdi1p is provided in substantial excess over requirements of wild-type strains.

These observations appear at odds with the fact that Pdi1p overexpression can enhance secretion of a variety of recombinant proteins (14, 47). Our quantitative model predicts that 10-fold elevation in the steady-state levels of Pdi1p should only increase the capacity of the OPF pathway by 1.4 fold, whereas similar overexpression of Ero1p should more than double the capacity of the pathway (**Figure 9**). Thus, manipulating Ero1p levels might provide a more promising strategy compared to manipulating Pdi1p levels. A number of studies have indeed shown that Ero1p overexpression can improve production of a range of recombinant substrates, from single chain variable fragments (scFv) to T-cell receptors, and for some substrates including different scFvs, Ero1p overexpression was indeed more beneficial than Pdi1p overexpression (61). Similarly, de Ruijter *et al.* (45) showed that increasing levels of Ero1p consistently enhanced titres of an antibody product expressed in yeast more than matched increases in levels of Pdi1p (45). However, these studies also demonstrate significant variability and substrate specificity in the behaviour of different recombinant products. It is likely that target recombinant mammalian proteins will have

evolved in the significantly more complex environment of the mammalian OPF pathway and may interact sub-optimally with yeast Pdi1p. This may explain why in some cases, individual substrates respond well to Pdi1p overexpression.

In conclusion, we have developed a novel method for the processing of Ero1p which enables, for the first time, an understanding of the *in vitro* concentration dependencies of the Pdi1p/Ero1p catalytic cycle. Based on a suite of biochemical assays, we generated a detailed computational model which accurately describes the interaction of Pdi1p and Ero1p for the oxidation of substrates. This model gives new insights into the yeast OPF and should form a platform on which to design future engineering strategies to enhance the secretion of authentic high value recombinant proteins from *S. cerevisiae.*

Innovation

Oxidative protein folding in eukaryotes utilises two proteins, PDI and ERO, to generate correctly positioned disulfide bonds. Using an advanced *in vitro* refolding process to isolate functional recombinant yeast ERO (Ero1p), we carried out the first quantitative assessment of the rates of PDI/ERO oxidation by oxygen. Based on these quantitative data we developed an ODE-based model of the oxidising capabilities of the yeast ER *in vivo*. This model gives new insights into native yeast OPF and suggests that engineering strategies to enhance the secretion of authentic high value recombinant proteins from yeast need to consider an expanded parameter space comprising both Pdi1p and Ero1p, depending on the efficiency with which Pdi1p and the recombinant substrate interact.

Materials and Methods

Plasmid construction

The plasmid encoding a codon optimised version of $Ero1p_{19\text{-}424}$ was a kind gift from Lloyd Ruddock (University of Oulu). The plasmid expressing yeast $Pdi1p_{22\text{-}530}$ without its N-terminal signal sequence was produced by PCR amplification of the relevant *PDI1* sequence from plasmid pUKC470 using a forward primer (GCGATGCATCACCATCACCACCATATGCAACAAGAGGCTGTGGCC) and a reverse primer

(CGCGCGGGATCCCGCTATTACAATTCATCGTGAATGGCATCTTCTTC) followed by digestion using *Nsi*I and *Bam*HI (Promega, Madison, Wisconsin) and ligation into a pET15b vector.

Protein Production

Pdi1p- and Ero1p-encoding plasmids were transformed into the BL21 [DE3] pLysS strain of *E. coli* (Invitrogen, Carlsbad, California) by heat shock at 42^{o}C for 60 sec. Transformants were selected by growth on LB agar plates containing 35 μg/ml chloramphenicol (Sigma Aldrich, St Louis, Missouri), and 100 μg/ml ampicillin (Sigma Aldrich, St Louis, Missouri). Individual transformed colonies were used to inoculate 10 ml of LB containing 35 μg/ml chloramphenicol and 100 μg/ml ampicillin and then grown overnight at 37^{o}C. The resulting cultures were centrifuged at 4000 rpm, the supernatant removed, the resulting cell pellet resuspended in 1 ml of LB and then used to inoculate 1 L of LB containing 35 μg/ml chloramphenicol and 100 μg/ml ampicillin. The cultures were grown to an OD_{600} of 0.6 before gene expression was induced as follows. Pdi1p synthesis was induced by 1 mM Isopropyl β-D-thiogalactopyranoside (IPTG) (Melford Laboratories, Ipswich, Suffolk) and incubated for 4 hours at 30^{o}C. Ero1p synthesis was induced by addition of 1 mM IPTG and 10 μM FAD (Sigma Aldrich, St Louis, Missouri) followed by incubation at 20^{o}C for 12-16 hr. The cells were harvested by centrifugation at 4,000 rpm for 10 mins before resuspension in 20 mM phosphate, 50 mM NaCl, pH7.4 plus protease inhibitor cocktail (Sigma Aldrich, St Louis, Missouri).

Protein Purification: Ero1p

Cells producing Ero1p were disrupted by sonication and the resulting lysate was treated with 2 M $MgCl_2$ (10 mM final concentration) and DNase A (150 U/L culture) (Sigma Aldrich, St Louis, Missouri) and incubated for 30 mins at room temperature. The resulting lysate was clarified by centrifugation at 27,216 xg for 30 mins at 4^{o}C. The supernatant was removed and treated with 5 M NaCl and 1 M imidazole to give 0.5 M and 10 mM concentrations respectively before incubation with Ni-NTA resin formed from chelating sepharose (2 ml of resin per 1 L of culture purified) (GE Healthcare, Chicago, Illinois) for 1 hour at room temperature. The resin was collected and washed with 10ml 20 mM phosphate, 50 mM NaCl, 10 mM imidazole, pH7.4 and then 10ml 20 mM phosphate, 50

mM NaCl, pH7.4 before elution of bound proteins with 1ml fractions of 20 mM phosphate, 50 mM NaCl, 50 mM EDTA, pH7.4. The resulting solution was diluted to 100 µM protein concentration before being treated with 30 mM DTT (Melford Laboratories, Ipswich, Suffolk) and incubated at room temperature for 1 hour. Any precipitated material was removed by centrifugation at 13000 rpm for 10 minutes prior to DTT removal by buffer exchange with PD10 cartridges (GE Healthcare, Chicago, Illinois) equilibrated with 20 mM phosphate, 50 mM NaCl, pH7.4. The approximate protein concentration was determined by absorbance at 280 nm before a 10-fold molar excess of FAD (~750 µM) was added to the mixture and incubated for 12-16 hr at room temperature. The mixture was concentrated using a 10 kDa MWCO (Pall, New York) centrifugal filter before loading onto a Superdex 200 16/600 gel column (GE Healthcare, Chicago, Illinois) equilibrated with 20 mM phosphate, 50 mM NaCl, pH7.4. The appropriate fractions were collected, protein concentration determined in the presence of 0.1% SDS to determine protein:FAD ratio, aliquoted and stored at -80^{o}C.

Protein Purification: Pdi1p

The Pdi1p purification protocol was based on the one described by Lappi & Ruddock (32). Briefly: cells producing Pdi1p were lysed by incubation at room temperature in the presence of 0.5% (v/v) Triton X-100 and a combination of DNase A (150 U/L culture) and $MgCl_2$ (10 mM) for 30 mins. The resulting lysate was clarified by centrifugation at 15,000 rpm for 30 mins at 4^{o}C and then incubated with Ni-NTA (1 ml/L culture) for 2 hr at room temperature. The resin was then collected and washed with 10ml 20 mM phosphate, 50 mM NaCl, 10 mM imidazole, pH7.4 and then 10ml 20 mM phosphate, 50 mM NaCl, pH7.4. The bound protein was eluted using 1ml fractions of 20 mM phosphate, 50 mM NaCl, 50 mM EDTA, pH7.4 and then buffer exchanged into 20 mM phosphate, 50 mM NaCl, pH7.4 using a PD10 column. The resulting mixture was purified using a 5 ml HiTrap Q FF anion exchange column (GE Healthcare, Chicago, Illinois) with a non-linear gradient between 20 mM phosphate, 50 mM NaCl, pH7.4 (Buffer A) and 20 mM phosphate, 1 M NaCl, pH7.4 (Buffer B) (Post injection 12ml buffer A, 2ml 0-20% B, 20ml 20-75% B, 15ml 75-100% B and 10ml 100% B). The appropriate fractions were then combined and concentrated using a 10 kDa MWCO centrifugal filter before aliquoting at freezing at -20^{o}C.

Preparation of reduced and denatured RNase A (rdRNase A)

Bovine pancreatic RNase A (Sigma Aldrich, St Louis, Missouri) was dissolved in 20 mM phosphate, 8 M Urea, pH8 to a concentration of ~750 µM and then treated with DTT at a final concentration of 30 mM. The reaction was incubated for 4 hrs at room temperature before quenching the reaction by lowering the pH to 3 with acetic acid. The buffer was then exchanged to 0.1 M acetic acid (AcOH) using PD10 columns. The protein concentration was determined and samples aliquoted before lyophilisation to dryness.

Oxygen consumption assay

Oxygen consumption was measured using a Clarke O_2 electrode (Rank Brothers, Bottisham, Cambridge, DM10) in conjunction with a Pico Technologies Data Logger and PicoLog software (Pico Technologies, St Neots, Cambridgeshire). A 1 ml chamber was utilised with a final reaction volume of 600 µl was used for each experiment.

Glutathione (GSH)-mediated oxygen consumption assay

Stock solutions of GSH (Sigma Aldrich, St Louis, Missouri) were prepared fresh before the start of every experiment and stored on ice. The thiol concentration of these stock solutions was calculated using Ellman's assay (11) and this concentration used to determine the volume to be added to give 40 mM GSH in the electrochemical cell.

Purified Pdi1p was combined with 10x O_2 consumption buffer (1 M Tris-HAc, 500 mM NaCl, pH8), H_2O and GSH (40 mM) and the baseline O_2 level allowed to stabilise for 100 secs before addition of Ero1p to the electrochemical cell.

Dithiothreitol (DTT)- mediated oxygen consumption assay

Purified Ero1p (1 µM) was combined with 10x O_2 consumption buffer and H_2O and the baseline O_2 level allowed to stabilise for 100 secs prior to addition of 1 M DTT.

Analysis of RNase A oxidation by 4-acetamido-4'-maleimidylstilbene-2,2'-disulfonic acid (AMS) trapping

Lyophilised reduced and denatured RNase A was dissolved in 0.1 M AcOH to 765 µM. Purified Pdi1p, 10x O_2 consumption buffer, H_2O and RNase A (60 µM) (Sigma Aldrich, St Louis, Missouri), were combined and the baseline O_2 level allowed to stabilise for 100 secs prior to addition of purified Ero1p (variable µM). Over the duration of the experiment 10 µl aliquots were removed from the electrochemical cell and quenched by the addition of 10 mM AMS (Molecular Probes, Invitrogen, Carlsbad, California) to give final concentration of 1 mM. The samples were incubated for 1 hr before treatment with 4 x SDS PAGE loading dye + 5% (v/v) 2-mercaptoethanol (Sigma Aldrich, St Louis, Missouri) and then heated to 95^{o}C for 5 minutes. 3 µl of each sample were run on a 15% Tris-Gly SDS PAGE at 180 V and then stained with Instant Blue (Expedeon, Over, Cambridge) stain. The resulting gels were scanned using an Epson Perfection 3200 flatbed scanner and band analysis carried out using ImageJ software (46).

In vitro Analysis of Pdi1p oxidation state by PEG trapping

600 µl O_2 consumption assays as described above, with rdRNase A as an electron source and varying Pdi1p and Ero1p concentrations, were analysed. At different time points 10 µl samples were removed from the electrode chamber and trapped by the addition of 1 µl 200 mM 5k PEG maleimide solution (Sigma Aldrich, St Louis, Missouri). The sample was thoroughly mixed and incubated for at least 30 min prior to the addition of 4 x SDS-PAGE loading buffer incorporating 5% (v/v) 2-mercaptoethanol. The samples were then boiled at 95^{o}C and analysed using SDS-PAGE and western blot. Polyclonal antibodies were raised in rabbit against purified Pdi1p and were produced by Capra Science (Ängelholm, Sweden).

In vivo analysis of Pdi1p oxidation state by PEG trapping

To allow for regulation of the expression of the *PDI1* gene, the tet-O promoter was introduced into the yeast strain R1158 in place of the native *PDI1* gene promoter. This strain enabled knockdown of *PDI1* expression and was constructed using the KanMX4-tetO cassette method developed by Yen *et al* (64). The resulting strain was named tet-*pdi1*. Overnight cultures of R1158 and tet-*pdi1* were re-inoculated to an OD_{600} of 0.2 in fresh

YEPD (2% w/v glucose, 1% w/v yeast extract and 2% w/v bactopeptone) and grown for 6 hr in the absence or presence of doxycycline (Sigma Aldrich, St Louis, Missouri) added to a final concentration of either 0.02 μg/ml (45 nM) or 0.1 μg/ml (225 nM). After 6 hr 5 OD_{600} units of cells were harvested at 16,100 *xg* and proteins were extracted in cell lysis buffer (1 x PBS, 100 mM NaCl, 100 mM EDTA pH 8.0, 1x protease inhibitor cocktail tablet) with or without 20 mM 5k PEG maleimide using glass bead lysis. Proteins were analysed using reducing SDS-PAGE and western blot analysis. Polyclonal antibodies were raised in rabbit against purified Pdi1p and were produced by Capra Science (Ängelholm, Sweden).

Computational modelling of oxygen consumption

An SBML version of the model file is available from the Biomodels database (www.ebi.ac.uk/biomodels (17)) under accession number MODEL1902080001. The fitting of experimental data to reactions was achieved using the COPASI 4.18 Parameter Estimation module (21). The average O_2 consumption data was calculated for each Pdi1p and Ero1p concentration variable with the 100 sec of baseline stabilisation time removed. Each change in parameter was accompanied by 10 repeats of the fitting to determine reproducibility of the fits in terms of the derived k value.

To compare between each run the average root-mean-squared-deviation (RMSD) for each experiment was calculated by averaging the values for each of the individual protein concentration variables obtained in each run. The rank order of fitting was defined by the lowest to highest RMSD value.

Estimation of protein oxidation rates in yeast in vivo

The main data source to identify proteins passing through the ER was Wiederhold et al. (63), who review and summarise information on mass spectrometry-based sub-cellular localisation experiments from 18 different pre-2010 studies. A number of later studies (15, 23, 51, 60) were used to complete this set.

Abundance data for each protein were used as reported in Ho *et al.* (20), protein half-life data were from Christiano *et al.* (9), and a doubling time was assumed of 120 minutes.

Abundance, decay-rate and number of cysteines per protein are listed in supplemental file S8. The maximum number of disulfide bonds to be formed per minute was calculated as

$$k_{cys} = \sum_{i=1}^{n} A_i \cdot \left\lfloor \frac{Cys_i}{2} \right\rfloor \cdot \left(k_i + \frac{ln(2)}{t_d} \right)$$

where A_i is the abundance of the *i*th protein and Cys_i is the number of cysteines it contains, k_i its degradation rate, and t_d the doubling time of the growing culture. The equation is based on the standard maths for first order reactions, assuming that in the steady state proteins need to be formed with a rate that balances their decay and their dilution through growth. It is assumed that only even numbers of cysteines can be oxidised.

Acknowledgements

The work reported in this paper was supported by a project grant from the Biotechnology and Biological Sciences Research Council (BBSRC, ref. no. BB/M009815/1). We would like to thank Richard Williamson (Kent) and Lloyd Ruddock (Oulu) for advice and the provision of key reagents. We dedicate this manuscript to the memory of our dear friend and collaborator Robert Freedman without whom none of the work reported here would have been possible.

Authors' Contributions

DMB, GLS and ELB performed the experiments; DMB, ELB, RBF, TvdH and MFT designed the research, analyzed the data and wrote the article.

Author Disclosure Statement

No competing financial interests exist.

REFERENCES

1. **Appenzeller-Herzog C**, **Riemer J**, **Christensen B**, **Sørensen ES**, **Ellgaard L**. A novel disulphide switch mechanism in Ero1alpha balances ER oxidation in human cells. *EMBO J* 27: 2977–2987, 2008.

2. **Appenzeller-Herzog C**, **Riemer J**, **Zito E**, **Chin K-T**, **Ron D**, **Spiess M**, **Ellgaard L**. Disulphide production by Ero1α-PDI relay is rapid and effectively regulated. *EMBO J* 29: 3318–3329, 2010.

3. **Araki K**, **Iemura S**, **Kamiya Y**, **Ron D**, **Kato K**, **Natsume T**, **Nagata K**. Ero1-α and PDIs constitute a hierarchical electron transfer network of endoplasmic reticulum oxidoreductases. *J Cell Biol* 202: 861–74, 2013.

4. **Araki K**, **Nagata K**. Functional in vitro analysis of the ERO1 protein and protein-disulfide isomerase pathway. *J Biol Chem* 286: 32705–32712, 2011.

5. **Baker KM**, **Chakravarthi S**, **Langton KP**, **Sheppard AM**, **Lu H**, **Bulleid NJ**. Low reduction potential of Ero1alpha regulatory disulphides ensures tight control of substrate oxidation. *EMBO J* 27: 2988–2997, 2008.

6. **Bellí G**, **Garí E**, **Aldea M**, **Herrero E**. Functional analysis of yeast essential genes using a promoter-substitution cassette and the tetracycline-regulatable dual expression system. *Yeast* 14: 1127–1138, 1998.

7. **Benham AM**, **van Lith M**, **Sitia R**, **Braakman I**. Ero1-PDI interactions, the response to redox flux and the implications for disulfide bond formation in the mammalian endoplasmic reticulum. *Philos Trans R Soc Lond B Biol Sci* 368: 20110403, 2013.

8. **Chambers JE**, **Tavender TJ**, **Oka OBV**, **Warwood S**, **Knight D**, **Bulleid NJ**. The reduction potential of the active site disulfides of human protein disulfide isomerase limits oxidation of the enzyme by Ero1α. *J Biol Chem* 285: 29200–29207, 2010.

9. **Christiano R**, **Nagaraj N**, **Fröhlich F**, **Walther TC**. Global Proteome Turnover Analyses of the Yeasts *S. cerevisiae* and *S. pombe. Cell Rep* 9: 1959–1965, 2014.

10. **Chu Y**, **Yang C**, **Chen X**, **Zheng W**, **Yang Y**, **Tang Y**. Structure–function analysis of human protein Ero1-Lα. *Biochem Biophys Res Commun* 389: 645–650, 2009.

11. **Ellman GL**. Tissue sulfhydryl groups. *Arch Biochem Biophys* 82: 70–77, 1959.

12. **Elsutohy MM**, **Chauhan VM**, **Markus R**, **Kyyaly MA**, **Tendler SJB**, **Aylott JW**. Real-time measurement of the intracellular pH of yeast cells during glucose metabolism using ratiometric fluorescent nanosensors. *Nanoscale* 9: 5904–5911, 2017.

13. **Farquhar R**, **Honey N**, **Murant SJ**, **Bossier P**, **Schultz L**, **Montgomery D**, **Ellis RW**, **Freedman RB**, **Tuite MF**. Protein disulfide isomerase is essential for viability in *Saccharomyces cerevisiae. Gene* 108: 81–9, 1991.

14. **Finnis CJA**, **Payne T**, **Hay J**, **Dodsworth N**, **Wilkinson D**, **Morton P**, **Saxton MJ**, **Tooth DJ**, **Evans RW**, **Goldenberg H**, **Scheiber-Mojdehkar B**, **Ternes N**, **Sleep D**. High-level production of animal-free recombinant transferrin from *Saccharomyces cerevisiae*. *Microb Cell Fact* 9: 87, 2010.

15. **Forsmark A**, **Rossi G**, **Wadskog I**, **Brennwald P**, **Warringer J**, **Adler L**. Quantitative Proteomics of Yeast Post-Golgi Vesicles Reveals a Discriminating Role for Sro7p in Protein Secretion. *Traffic* 12: 740–753, 2011.

16. **Frand AR**, **Kaiser CA**. The ERO1 gene of yeast is required for oxidation of protein dithiols in the endoplasmic reticulum. *Mol Cell* 1: 161–170, 1998.

17. **Glont M**, **Nguyen TVN**, **Graesslin M**, **Hälke R**, **Ali R**, **Schramm J**, **Wimalaratne SM**, **Kothamachu VB**, **Rodriguez N**, **Swat MJ**, **Eils J**, **Eils R**, **Laibe C**, **Malik-Sheriff RS**, **Chelliah V**, **Le Novère N**, **Hermjakob H**. BioModels: expanding horizons to include more modelling approaches and formats. *Nucleic Acids Res* 46: D1248–D1253, 2018.

18. **Gross E**, **Kastner DB**, **Kaiser CA**, **Fass D**. Structure of Ero1p, source of disulfide bonds for oxidative protein folding in the cell. *Cell* 117: 601–10, 2004.

19. **Gross E**, **Sevier CS**, **Heldman N**, **Vitu E**, **Bentzur M**, **Kaiser CA**, **Thorpe C**, **Fass D**. Generating disulfides enzymatically: reaction products and electron acceptors of the

endoplasmic reticulum thiol oxidase Ero1p. *Proc Natl Acad Sci U S A* 103: 299–304, 2006.

20. **Ho B**, **Baryshnikova A**, **Brown GW**. Unification of Protein Abundance Datasets Yields a Quantitative *Saccharomyces cerevisiae* Proteome. *Cell Syst* 6: 192–205, 2018.

21. **Hoops S**, **Sahle S**, **Gauges R**, **Lee C**, **Pahle J**, **Simus N**, **Singhal M**, **Xu L**, **Mendes P**, **Kummer U**. COPASI--a COmplex PAthway SImulator. *Bioinformatics* 22: 3067–74, 2006.

22. **Horton LE**, **James P**, **Craig E a**, **Hensold JO**. The yeast hsp70 homologue Ssa is required for translation and interacts with Sis1 and Pab1 on translating ribosomes. *J Biol Chem* 276: 14426–14433, 2001.

23. **Hsu P-H**, **Chiang P-C**, **Liu C-H**, **Chang Y-W**. Characterization of Cell Wall Proteins in *Saccharomyces cerevisiae* Clinical Isolates Elucidates Hsp150p in Virulence. *PLoS One* 10: e0135174, 2015.

24. **Hwang C**, **Sinskey AJ**, **Lodish HF**. Oxidized redox state of glutathione in the endoplasmic reticulum. *Science* 257: 1496–1502, 1992.

25. **Inaba K**, **Masui S**, **Iida H**, **Vavassori S**, **Sitia R**, **Suzuki M**. Crystal structures of human Ero1α reveal the mechanisms of regulated and targeted oxidation of PDI. *EMBO J* 29: 3330–3343, 2010.

26. **Kakihana T**, **Nagata K**, **Sitia R**. Peroxides and peroxidases in the endoplasmic reticulum: integrating redox homeostasis and oxidative folding. *Antioxid Redox Signal* 16: 763–771, 2012.

27. **Kanemura S**, **Okumura M**, **Yutani K**, **Ramming T**, **Hikima T**, **Appenzeller-Herzog C**, **Akiyama S**, **Inaba K**. Human ER Oxidoreductin-1α (Ero1α) Undergoes Dual Regulation through Complementary Redox Interactions with Protein-Disulfide Isomerase. *J Biol Chem* 291: 23952–23964, 2016.

28. **Kim S**, **Sideris DP**, **Sevier CS**, **Kaiser CA**. Balanced Ero1 activation and inactivation establishes ER redox homeostasis. *J Cell Biol* 196: 713–725, 2012.

29. **Kimura T**, **Nishida A**, **Ohara N**, **Yamagishi D**, **Horibe T**, **Kikuchi M**. Functional analysis of the CXXC motif using phage antibodies that cross-react with protein disulphide-isomerase family proteins. *Biochem J* 382: 169–176, 2004.

30. **Kulp MS**, **Frickel E-M**, **Ellgaard L**, **Weissman JS**. Domain architecture of protein-disulfide isomerase facilitates its dual role as an oxidase and an isomerase in Ero1p-mediated disulfide formation. *J Biol Chem* 281: 876–884, 2006.

31. **LaMantia ML**, **Lennarz WJ**. The essential function of yeast protein disulfide isomerase does not reside in its isomerase activity. *Cell* 74: 899–908, 1993.

32. **Lappi A-K**, **Ruddock LW**. Reexamination of the Role of Interplay between Glutathione and Protein Disulfide Isomerase. *J Mol Biol* 409: 238–249, 2011.

33. **Llopis J**, **McCaffery JM**, **Miyawaki A**, **Farquhar MG**, **Tsien RY**. Measurement of cytosolic, mitochondrial, and Golgi pH in single living cells with green fluorescent proteins. *Proc Natl Acad Sci U S A* 95: 6803–6808, 1998.

34. **Masui S**, **Vavassori S**, **Fagioli C**, **Sitia R**, **Inaba K**. Molecular bases of cyclic and specific disulfide interchange between human ERO1alpha protein and protein-disulfide isomerase (PDI). *J Biol Chem* 286: 16261–16271, 2011.

35. **Montero D**, **Tachibana C**, **Rahr Winther J**, **Appenzeller-Herzog C**. Intracellular glutathione pools are heterogeneously concentrated. *Redox Biol* 1: 508–513, 2013.

36. **Nguyen VD**, **Saaranen MJ**, **Karala A-R**, **Lappi A-K**, **Wang L**, **Raykhel IB**, **Alanen HI**, **Salo KEH**, **Wang C-C**, **Ruddock LW**. Two endoplasmic reticulum PDI peroxidases increase the efficiency of the use of peroxide during disulfide bond formation. *J Mol Biol* 406: 503–15, 2011.

37. **Niu Y**, **Zhang L**, **Yu J**, **Wang C-C**, **Wang L**. Novel Roles of the Non-catalytic Elements of Yeast Protein-disulfide Isomerase in Its Interplay with Endoplasmic Reticulum Oxidoreductin 1. *J Biol Chem* 291: 8283–8294, 2016.

38. **Nørgaard P**, **Westphal V**, **Tachibana C**, **Alsøe L**, **Holst B**, **Winther JR**. Functional differences in yeast protein disulfide isomerases. *J Cell Biol* 152: 553–562, 2001.

39. **Paroutis P**, **Touret N**, **Grinstein S**. The pH of the Secretory Pathway: Measurement, Determinants, and Regulation. *Physiology* 19: 207–215, 2004.

40. **Payne T**, **Finnis C**, **Evans LR**, **Mead DJ**, **Avery S V**, **Archer DB**, **Sleep D**. Modulation of chaperone gene expression in mutagenized *Saccharomyces cerevisiae* strains developed for recombinant human albumin production results in increased production of multiple heterologous proteins. *Appl Environ Microbiol* 74: 7759–7766, 2008.

41. **Pollard MG**, **Travers KJ**, **Weissman JS**. Ero1p: a novel and ubiquitous protein with an essential role in oxidative protein folding in the endoplasmic reticulum. *Mol Cell* 1: 171–182, 1998.

42. **Ramming T**, **Appenzeller-Herzog C**. The physiological functions of mammalian endoplasmic oxidoreductin 1: on disulfides and more. *Antioxid Redox Signal* 16: 1109–18, 2012.

43. **Ramming T**, **Okumura M**, **Kanemura S**, **Baday S**, **Birk J**, **Moes S**, **Spiess M**, **Jenö P**, **Bernèche S**, **Inaba K**, **Appenzeller-Herzog C**. A PDI-catalyzed thiol-disulfide switch regulates the production of hydrogen peroxide by human Ero1. *Free Radic Biol Med* 83: 361–372, 2015.

44. **Robinson AS**, **Hines V**, **Wittrup KD**. Protein disulfide isomerase overexpression increases secretion of foreign proteins in *Saccharomyces cerevisiae*. *Bio/technology* 12: 381–384, 1994.

45. **de Ruijter JC**, **Koskela E V**, **Frey AD**. Enhancing antibody folding and secretion by tailoring the *Saccharomyces cerevisiae* endoplasmic reticulum. *Microb Cell Fact* 15: 87, 2016.

46. **Schindelin J**, **Arganda-Carreras I**, **Frise E**, **Kaynig V**, **Longair M**, **Pietzsch T**, **Preibisch S**, **Rueden C**, **Saalfeld S**, **Schmid B**, **Tinevez J-Y**, **White DJ**, **Hartenstein V**, **Eliceiri K**, **Tomancak P**, **Cardona A**. Fiji: an open-source platform for biological-image analysis. *Nat Methods* 9: 676–682, 2012.

47. **Schultz LD**, **Markus HZ**, **Hofmann KJ**, **Montgomery DL**, **Dunwiddie C**, **Kniskern PJ**, **Freedman RB**, **Ellis RW**, **TUITE MF**. Using Molecular Genetics to Improve the Production of Recombinant Proteins by the Yeast Saccharomyces cerevisiae. *Ann N Y Acad Sci* 721: 148–157, 1994.

48. **Schwaller M**, **Wilkinson B**, **Gilbert HF**. Reduction-Reoxidation Cycles Contribute to Catalysis of disulfide Isomerization by Protein-disulfide Isomerase. *J Biol Chem* 278: 7154–7159, 2003.

49. **Sevier CS**, **Qu H**, **Heldman N**, **Gross E**, **Fass D**, **Kaiser CA**. Modulation of cellular disulfide-bond formation and the ER redox environment by feedback regulation of Ero1. *Cell* 129: 333–344, 2007.

50. **Shepherd C**, **Oka OB V**, **Bulleid NJ**. Inactivation of mammalian Ero1α is catalysed by specific protein disulfide-isomerases. *Biochem J* 461: 107–113, 2014.

51. **Smeekens JM**, **Xiao H**, **Wu R**. Global Analysis of Secreted Proteins and Glycoproteins in *Saccharomyces cerevisiae*. *J Proteome Res* 16: 1039–1049, 2017.

52. **Tachibana C**, **Stevens TH**. The yeast *EUG1* gene encodes an endoplasmic reticulum protein that is functionally related to protein disulfide isomerase. *Mol Cell Biol* 12: 4601–4611, 1992.

53. **Tavender TJ**, **Springate JJ**, **Bulleid NJ**. Recycling of peroxiredoxin IV provides a novel pathway for disulphide formation in the endoplasmic reticulum. *EMBO J* 29: 4185–4197, 2010.

54. **Tu BP**, **Ho-Schleyer SC**, **Travers KJ**, **Weissman JS**. Biochemical basis of oxidative protein folding in the endoplasmic reticulum. *Science* 290: 1571–1574, 2000.

55. **Tu BP**, **Weissman JS**. The FAD- and O_2-dependent reaction cycle of Ero1-mediated oxidative protein folding in the endoplasmic reticulum. *Mol Cell* 10: 983–994, 2002.

56. **Tu BP**, **Weissman JS**. Oxidative protein folding in eukaryotes: mechanisms and consequences. *J Cell Biol* 164: 341–346, 2004.

57. **Vitu E**, **Kim S**, **Sevier CS**, **Lutzky O**, **Heldman N**, **Bentzur M**, **Unger T**, **Yona M**, **Kaiser CA**, **Fass D**. Oxidative activity of yeast Ero1p on protein disulfide isomerase and related oxidoreductases of the endoplasmic reticulum. *J Biol Chem* 285: 18155–18165, 2010.

58. **Wang L**, **Li S**, **Sidhu A**, **Zhu L**, **Liang Y**, **Freedman RB**, **Wang C**. Reconstitution of human Ero1-Lalpha/protein-disulfide isomerase oxidative folding pathway in vitro. Position-dependent differences in role between the a and a' domains of protein-disulfide isomerase. *J Biol Chem* 284: 199–206, 2009.

59. **Wang L**, **Zhang L**, **Niu Y**, **Sitia R**, **Wang C**. Glutathione Peroxidase 7 Utilizes Hydrogen Peroxide Generated by Ero1α to Promote Oxidative Protein Folding. *Antioxid Redox Signal* 20: 545–556, 2014.

60. **Wang X**, **Li S**, **Wang H**, **Shui W**, **Hu J**. Quantitative proteomics reveal proteins enriched in tubular endoplasmic reticulum of *Saccharomyces cerevisiae. Elife* 6: e23816, 2017.

61. **Wentz AE**, **Shusta E V.** A Novel High-Throughput Screen Reveals Yeast Genes That Increase Secretion of Heterologous Proteins. *Appl Environ Microbiol* 73: 1189–1198, 2007.

62. **West M**, **Zurek N**, **Hoenger A**, **Voeltz GK**. A 3D analysis of yeast ER structure reveals how ER domains are organized by membrane curvature. *J Cell Biol* 193: 333–346, 2011.

63. **Wiederhold E**, **Veenhoff LM**, **Poolman B**, **Slotboom DJ**. Proteomics of *Saccharomyces cerevisiae* Organelles. *Mol Cell Proteomics* 9: 431–445, 2010.

64. **Yen K**, **Gitsham P**, **Wishart J**, **Oliver SG**, **Zhang N**. An improved tetO promoter replacement system for regulating the expression of yeast genes. *Yeast* 20: 1255–1262, 2003.

65. **Young CL**, **Robinson AS**. Protein folding and secretion: mechanistic insights advancing recombinant protein production in *S. cerevisiae*. *Curr Opin Biotechnol* 30: 168–177, 2014.

66. **Zhang L**, **Niu Y**, **Zhu L**, **Fang J**, **Wang X**, **Wang L**, **Wang C**. Different interaction modes for protein-disulfide isomerase (PDI) as an efficient regulator and a specific substrate of endoplasmic reticulum oxidoreductin-1α (Ero1α). *J Biol Chem* 289: 31188–31199, 2014.

67. **Zito E**, **Melo EP**, **Yang Y**, **Wahlander Å**, **Neubert TA**, **Ron D**. Oxidative protein folding by an endoplasmic reticulum-localized peroxiredoxin. *Mol Cell* 40: 787–797, 2010.

Abbreviations

AcOH	Acetic acid
AMS	4-Acetamido-4'-Maleimidylstilbene-2,2'-Disulfonic Acid
COPASI	Complex Pathway Simulator
Cys	Cysteine
DNase A	Deoxyribonuclease A
DTT	1,4-Dithiothreitol
EDTA	Ethylenediaminetetraacetic acid
ER	Endoplasmic reticulum
ERO1	Endoplasmic reticulum oxidase 1
FAD	Flavin adenine dinucleotide
GSH	Glutathione
GSSG	Glutathione disulfide
H_2O_2	Hydrogen peroxide
$MgCl_2$	Magnesium chloride
MWCO	Molecular weight cut off
NaCl	Sodium chloride
NADPH	Nicotinamide adenine dinucleotide phosphate
Ni-NTA	Ni^{2+} loaded nitrilotriacetic acid modified sepharose
ODE	Ordinary Differential Equations
OPF	Oxidative Protein Folding
O_2	Oxygen
PCR	Polymerase chain reaction
PEG	Polyethylene glycol
PDI	Protein disulfide isomerase
rdRNase A	Reduced and denatured ribonuclease A
RNase A	Ribonuclease A
scFV	Single chain variable fragment antibody
SDS	Sodium dodecyl sulfate
SDS PAGE	Sodium dodecyl sulfate poly acrylamide gel electrophoresis

Tet	Tetracycline
Tris-HAc	Tris-acetic acid buffer
Tris-Gly	Tris-Glycine buffer

FIGURE LEGENDS

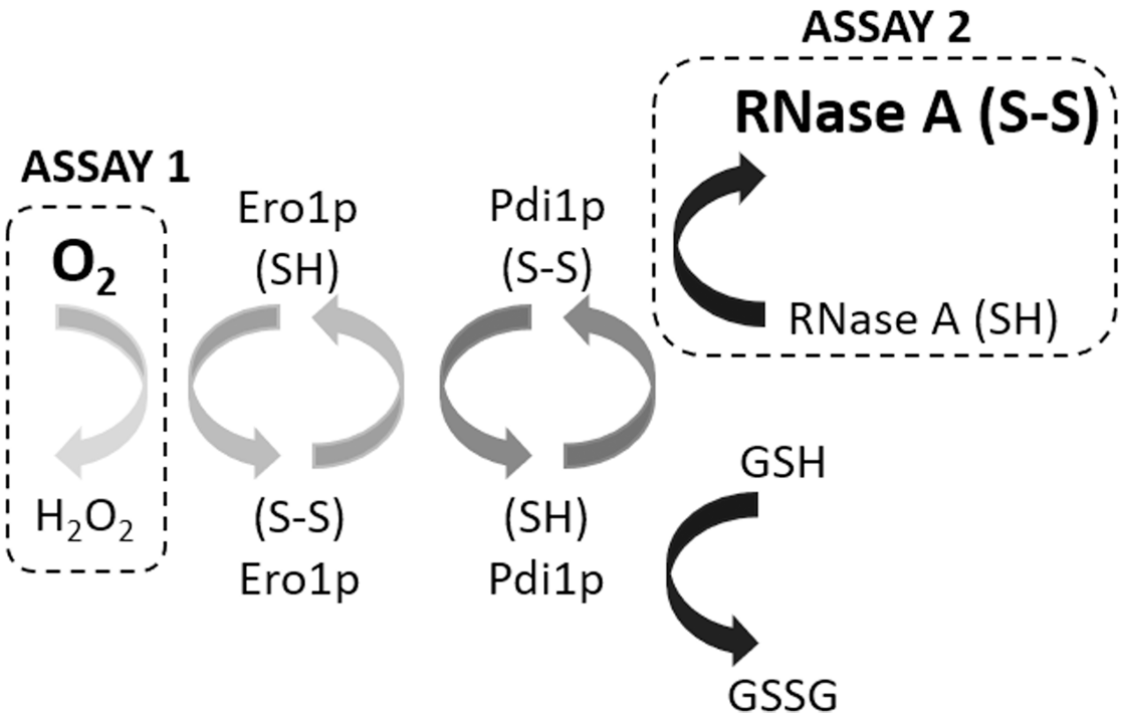

Figure 1: Methods for *in vitro* analysis of electron flow in the yeast OPF pathway. The ER oxidative folding pathway can be reconstituted with Ero1p and Pdi1p in the presence of dissolved O_2 as the terminal electron acceptor and either GSH (*Assay 1*) or reduced protein substrate (*Assay 2*) as the electron source. The operation of the pathway can be monitored either by the disappearance of O_2 (*Assay 1*), by the change in redox state of the substrate protein (*Assay 2*).

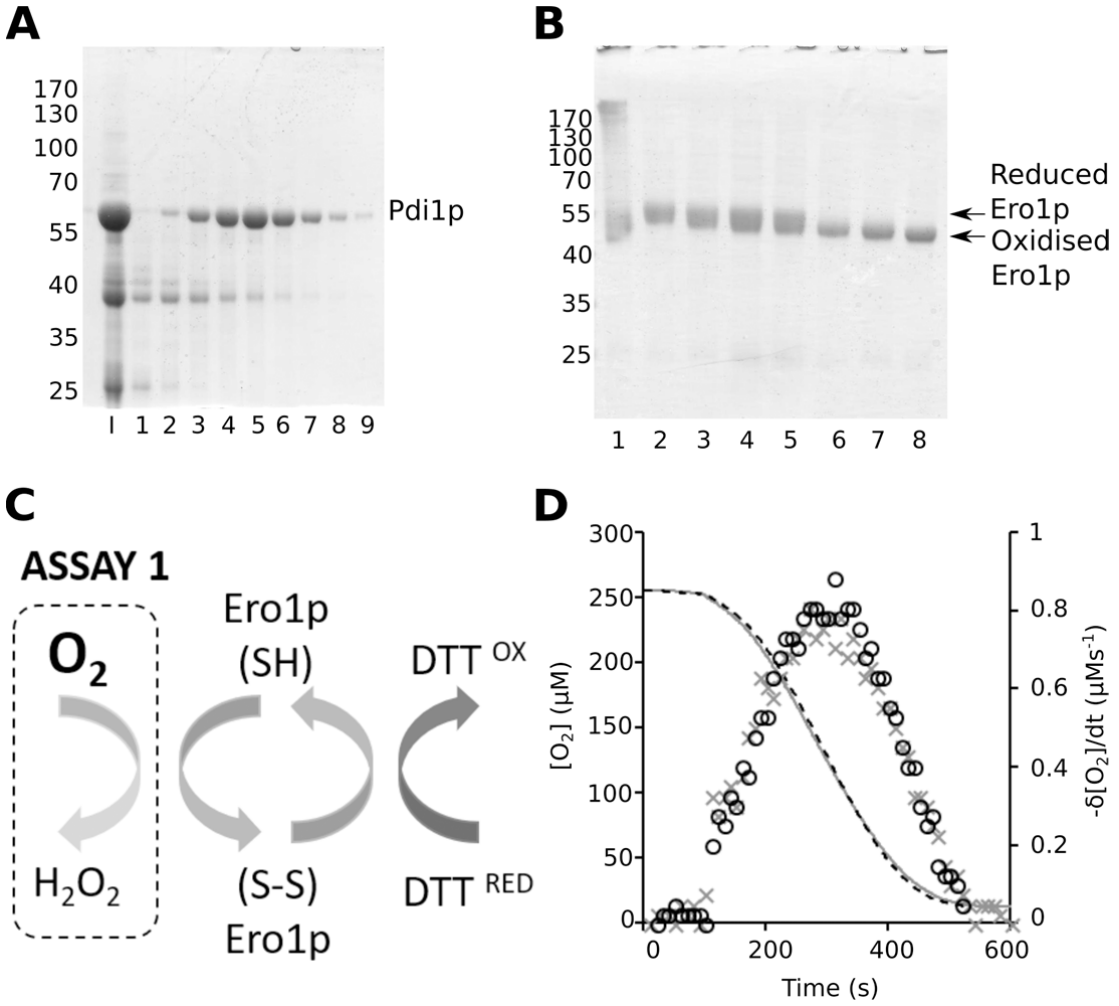

Figure 2: Purification of proteins for analysis of the yeast OPF pathway. (A): Reducing SDS-PAGE of Pdi1p purification (I) input, lanes 1-9; fractions from HiTrap Q FF purification. **(B)**: Reducing SDS-PAGE of Ero1p purification after AMS trapping: Lane 1, post Ni-NTA purification; lane 2, reduction of the Ni-NTA eluent by DTT (30 mM); lanes 3-6, reoxidation in the presence of FAD at 10 min, 30 min, 60 min and 18 hr; lane 7, purified Ero1p trapped with AMS; lane 8, purified Ero1p trapped with NEM. **(C)**: Schematic showing the Ero1p activity assay where Ero1p reduced by DTT is reoxidised by O_2, which is measurable using a Clarke electrode. (**D):** O_2 consumption assay using a Clarke electrode. 1 μM Ero1p equilibrated for 100 secs before addition of DTT (10 mM final concentration) to initiate Ero1p-mediated O_2 consumption (primary axis). The graph displays two replicates of the experiment. The non-linearity of O_2 consumption is shown by the increase in rate of reaction overtime to a maximum before decreasing again to 0 (secondary axis).

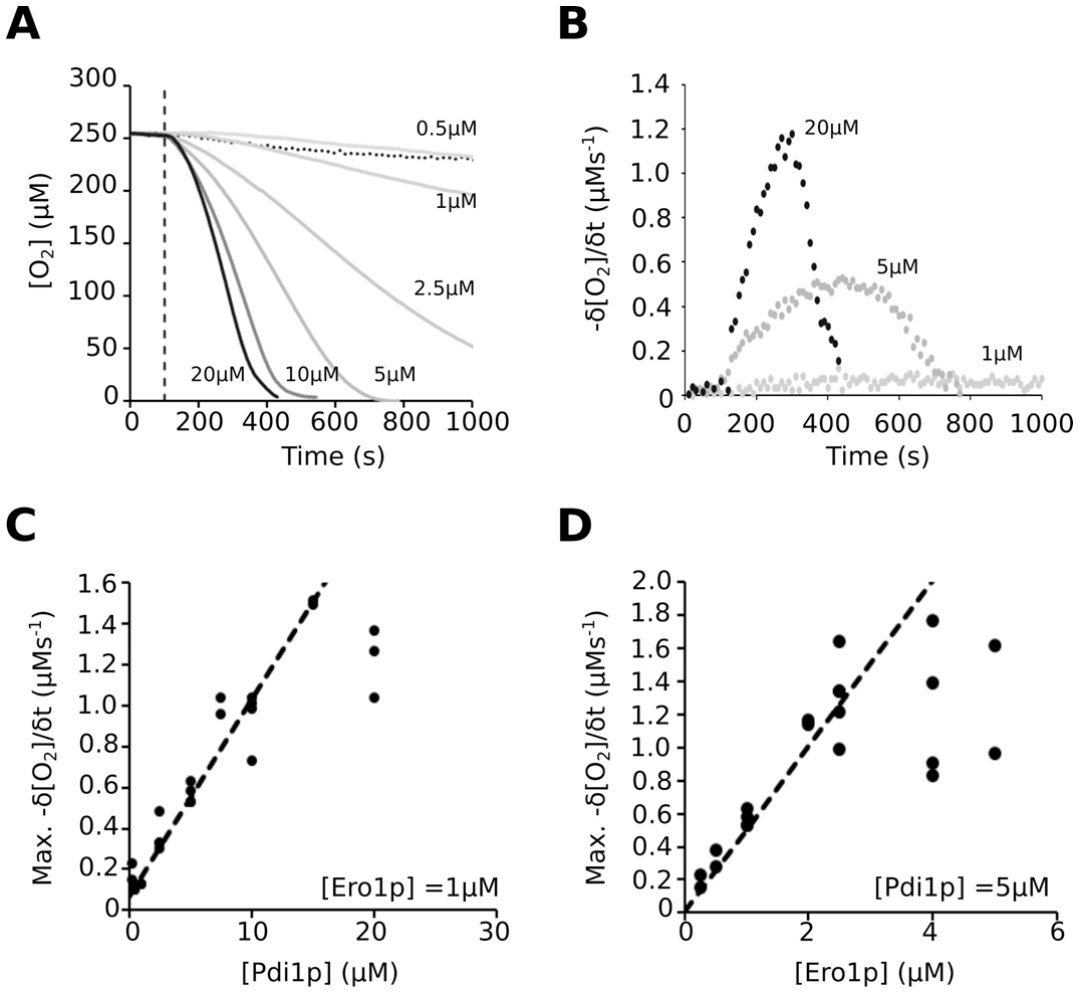

Figure 3: The oxidising activity of the yeast OPF pathway is dependent on the concentration of Pdi1p and Ero1p. (A) The O_2 consumed when variable concentrations of Pdi1p are reoxidised by Ero1p (1 μM) in the presence of 40 mM GSH. Buffer composition 100 mM Tris-AcOH, 50 mM NaCl, pH 8, 25^{o}C. All reagents except the Ero1p were combined and equilibrated, with constant stirring, to give a static baseline before Ero1p addition 100 sec after the initiation of the experiment. An average of at least two replicates is plotted. (**B)** The non-linearity of the observed O_2 consumption was assessed by determining the change in rate of O_2 consumption over the course of the experiment, using 10 sec intervals. Three representative curves are shown (20 μM, 5 μM and 1 μM) all exhibiting a slow increase in rate towards a maximum value before decreasing. (**C/D)** The extracted maximum rates of O_2 consumption for all repeats, as determined from the data in panel **B**, and plotted against enzyme concentration for Pdi1p (**C**) and Ero1p (**D**).

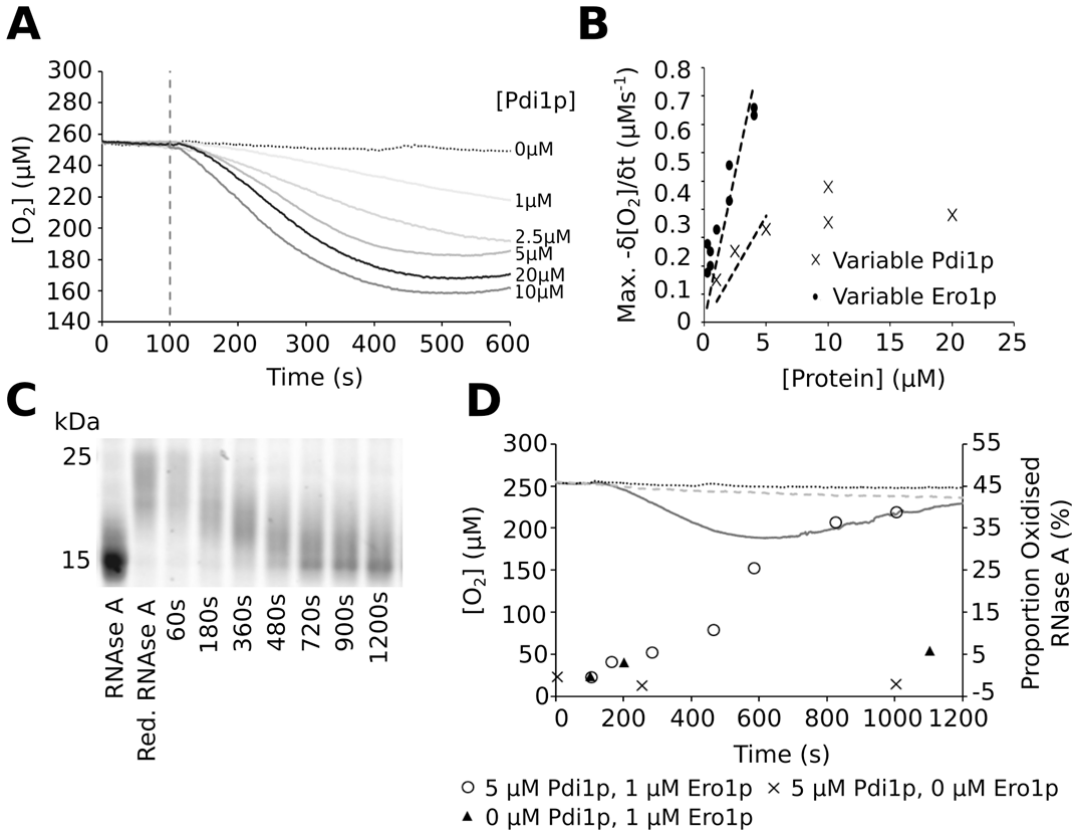

Figure 4: The interaction of Pdi1p and Ero1p mediates reoxidation of reduced and denatured RNase A. (A) O_2 consumption observed when 60 μM reduced and denatured RNase A added to Pdi1p and Ero1p. The concentration of Pdi1p was varied between 1 and 20 μM with a fixed Ero1p concentration of 1 μM. All reagents except Ero1p were combined and stirred at a constant speed for 100 secs prior to addition of Ero1p. **(B)** The maximum rate of O_2 consumption at different enzyme concentrations: variable Pdi1p with fixed [Ero1p] (1 μM) (dark grey x) and variable Ero1p with fixed [Pdi1p] (5 μM) (black filled circles ●). Data shown for all replicates. **(C)** 15% Tris-Gly SDS PAGE analysis of the Pdi1p (5 μM)/Ero1p (1 μM) mediated reoxidation of RNase A over-time using AMS trapping. **(D)** O_2 consumption for RNase A reoxidation. The primary axis, for 5 μM Pdi1p and 1 μM Ero1p (dark grey), no Pdi1p (dotted line) and no Ero1p (dashed line). The secondary axis shows the quantitation, by Image J, of the oxidised fraction from (**B**) over the course of the experiment. ▲– no Pdi1p, x – No Ero1p and o – 5 μM Pdi1p and 1 μM Ero1p.

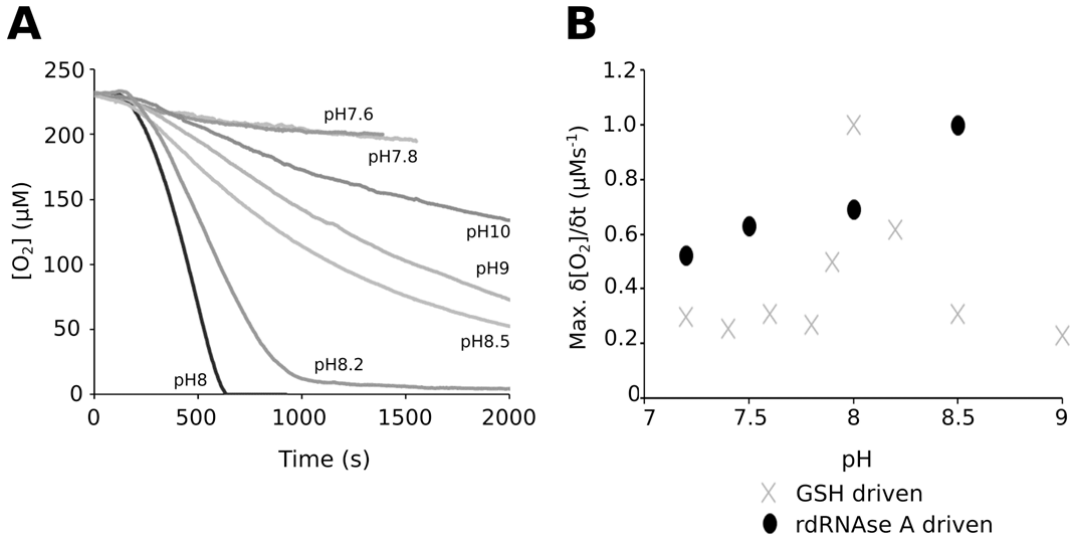

Figure 5: GSH-mediated Pdi1p/Ero1p interaction is pH regulated. (A) Oxygen consumption traces for 5 µM Pdi1p and 1 µM Ero1p when treated with 40 mM GSH under identical conditions except for variation of the reaction pH. **(B)** Comparison of the maximum rate of oxygen consumption at different pH values with either GSH (x) or reduced and denatured RNase A (●) as electron source.

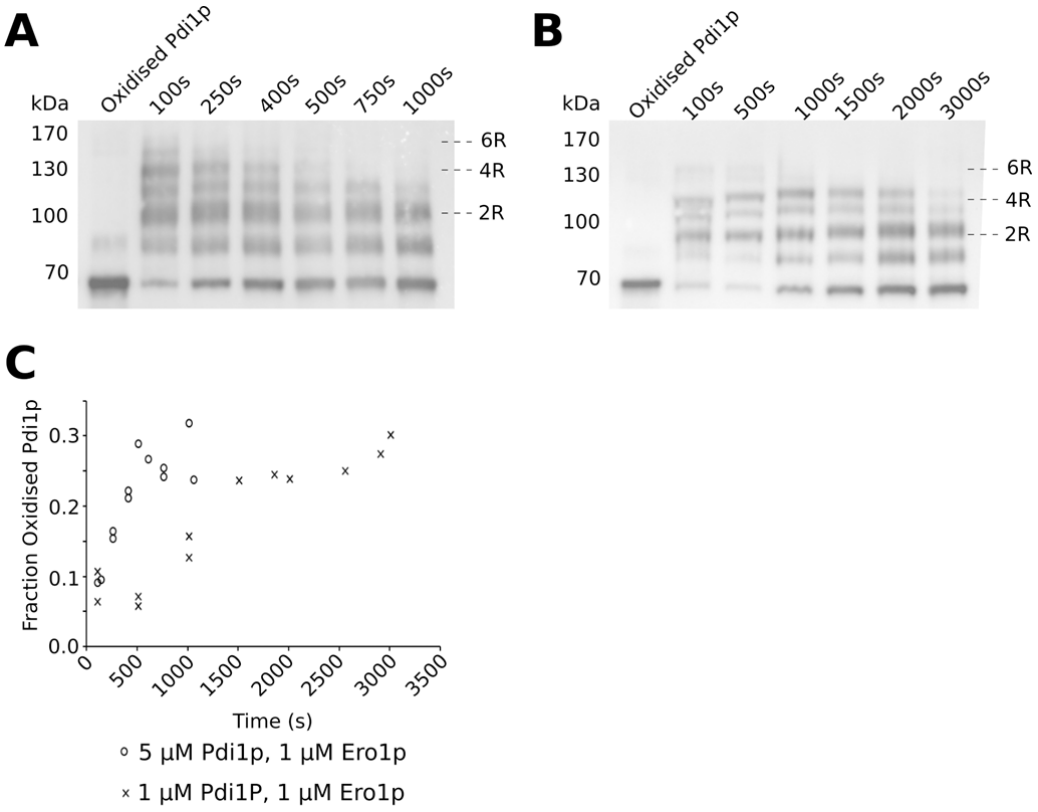

Figure 6: The bulk Pdi1p redox state remains reduced when it becomes the limiting component. (A) Anti-Pdi1p western blot showing the redox state of Pdi1p over the course of Ero1p-mediated RNase A (60 µM) reoxidation catalysed by 5 µM Pdi1p, 1 µM Ero1p. **(B)** Anti-Pdi1p western blot showing the redox state of Pdi1p over the course of Ero1p-mediated RNase A (60 µM) reoxidation catalysed by 1 µM Pdi1p, 1 µM Ero1p. **(C)** Densitometry analysis of the oxidised band over the course of the experiment for 5 µM Pdi1p, 1 µM Ero1p (o) and 1 µM Pdi1p, 1 µM Ero1p (x).

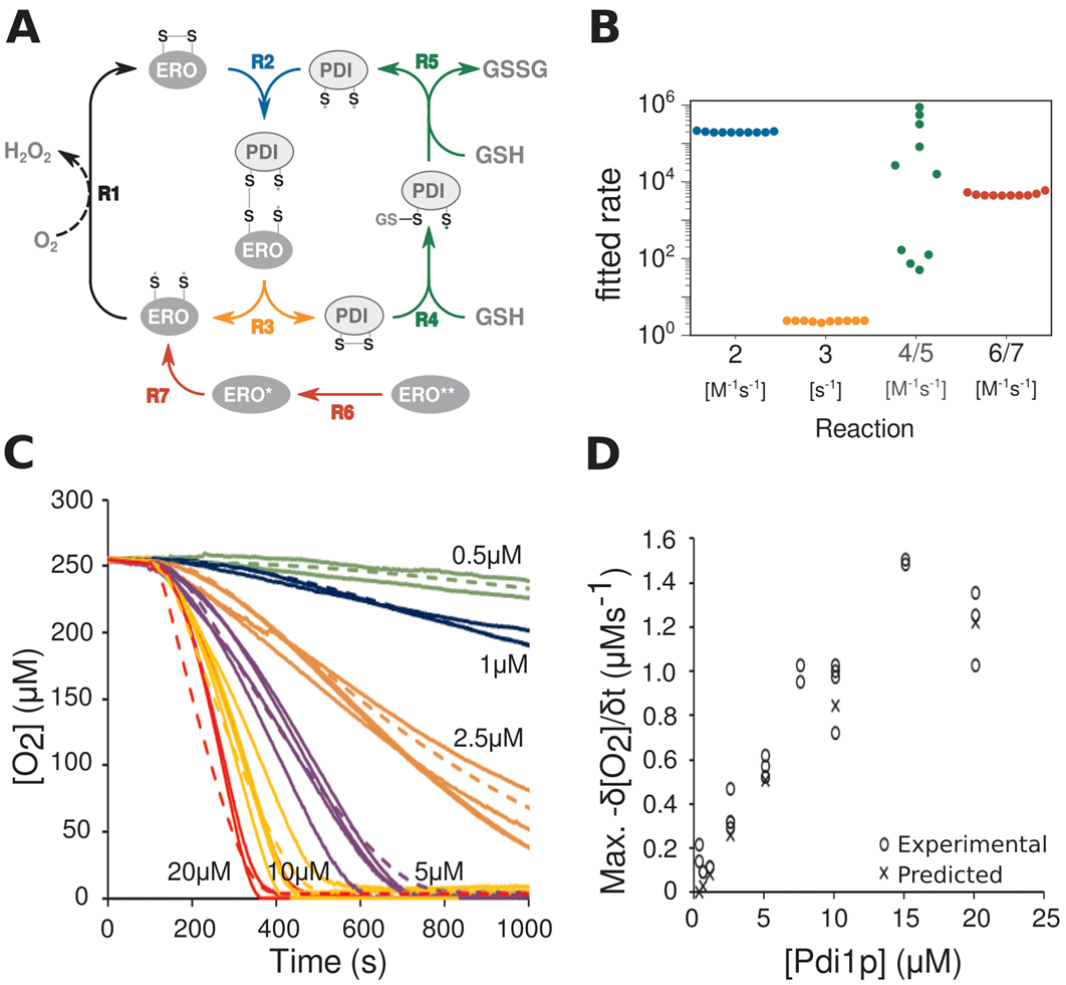

Figure 7: Kinetic Modelling of GSH-promoted Pdi1p/Ero1p interaction. (A) Representation of the model showing the reaction steps incorporated to define the electron transfer from GSH to molecular oxygen. **(B)** A comparison of 10 separate model repeats for each of the terms defined in (A). R1 was determined experimentally and was therefore not incorporated in the fitting. **(C)** The bulk experimental O_2 consumption data where the solid lines are colour coded to show [Pdi1p] compared to the O_2 consumption data generated by the best fitting data, dashed lines (- -), i.e. the best fitting data was that achieved using the parameters from the third of the ten modelling replicates observed in Fig. 6B. **(D)** Comparison of the experimentally observed (o) maximum for $\delta[O_2]/\delta t$ with that calculated using the data predicted (x) by the model.

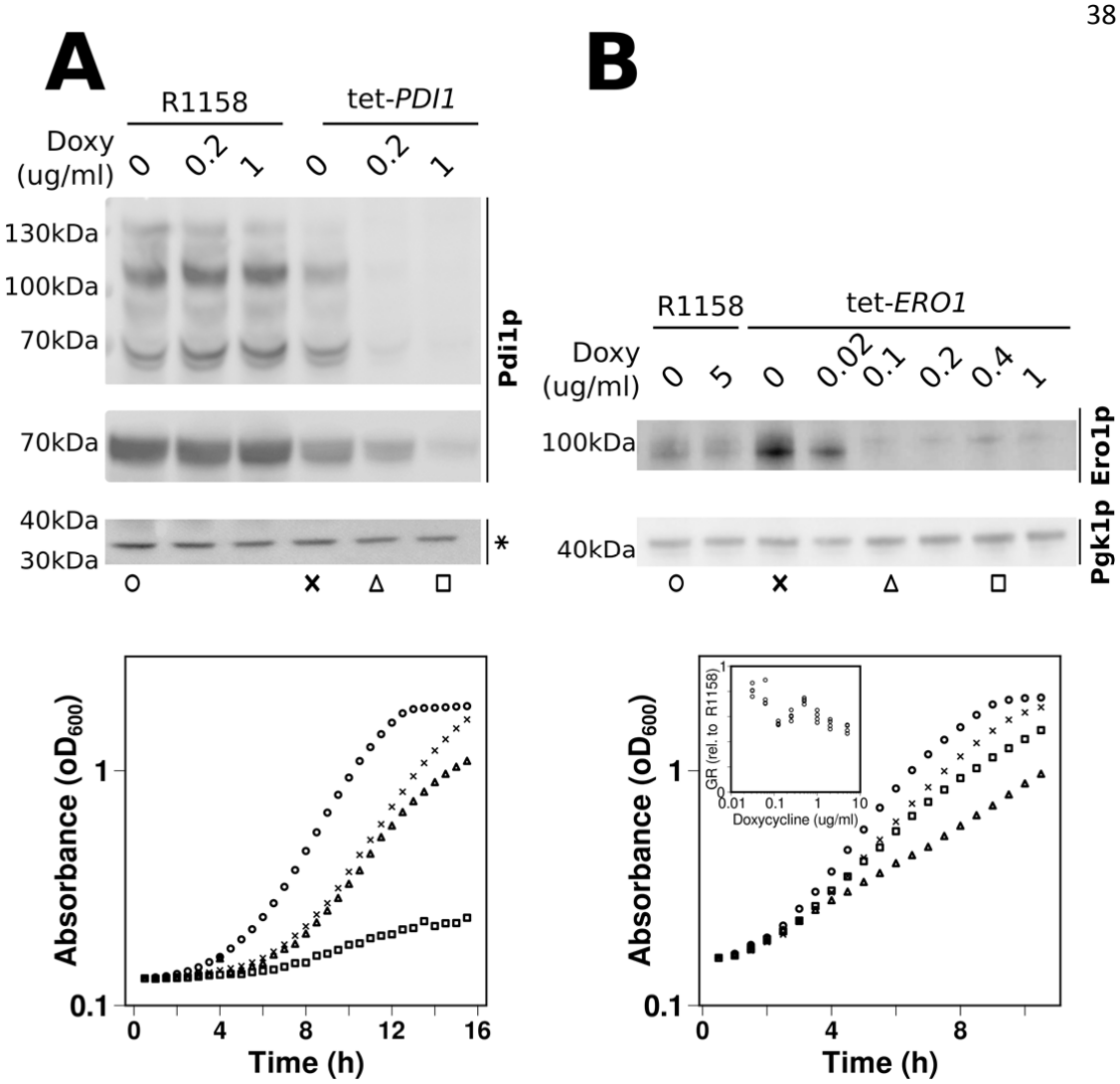

Figure 8: Yeast fitness correlates with intracellular levels of Pdi1p and Ero1p. This figure presents analyses of strains where expression of the *PDI1* or *ERO1* genes was place under control of a doxycycline-repressible promoter (Tet-Pdi1 and Tet-Ero1, respectively), compared to isogenic control strains containing the natural promoters (R1158). **(A) Top panel**: anti-Pdi1 western blots of samples treated with 5k PEG maleimide which shifts reduced Pdi1p to higher molecular weight, anti-Pdi1 western blots of non-PEG maleimide treated protein showing total Pdi1p content per cell, and loading controls for the Pdi1p western blots (a lower molecular weight non-specific band cross-reacting with the anti-Pdi1p antibody). **Bottom panel**: growth curves for selected strains and conditions, corresponding to symbols underneath the western blots. **(B) Top panel**: anti-Ero1 western blot of non-PEG-maleimide treated samples, and loading control (Pgk1p). **Bottom panel**:

growth curves for selected strains and conditions, corresponding to symbols underneath the blots. The inset graph shows growth rates of Tet-*ERO1* strains, expressed relative to the growth rate of R1158, for a wider range of doxycycline concentrations.

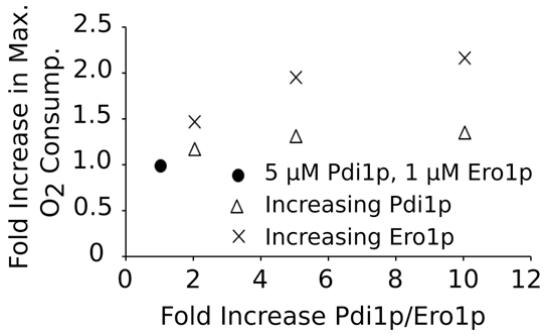

Figure 9: Predicted increase in oxidative folding capacity on Pdi1p/Ero1p overexpression. The increase in oxidative folding capacity of the Pdi1p/Ero1p system when the concentration of the OPF components are increased. ● 5 µM Pdi1p and 1 µM Ero1p; x = increase in Ero1.

Beal et al SUPPLEMENTARY FIGURE S1

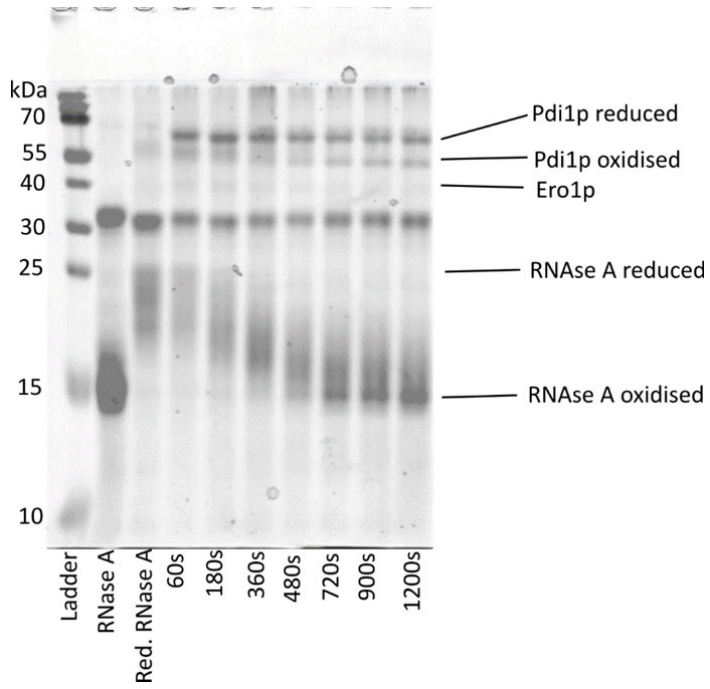

Figure S1. Full gel image of the data shown in Figure 4C. RNAse A reoxidation over time catalysed by 5 µM Pdi1p and 1 µM Ero1p was analysed by reducing SDS PAGE after AMS trapping. Pdi1p, Ero1p and RNAse A are marked on the gel.

Beal et al SUPPLEMENTARY FIGURE S2

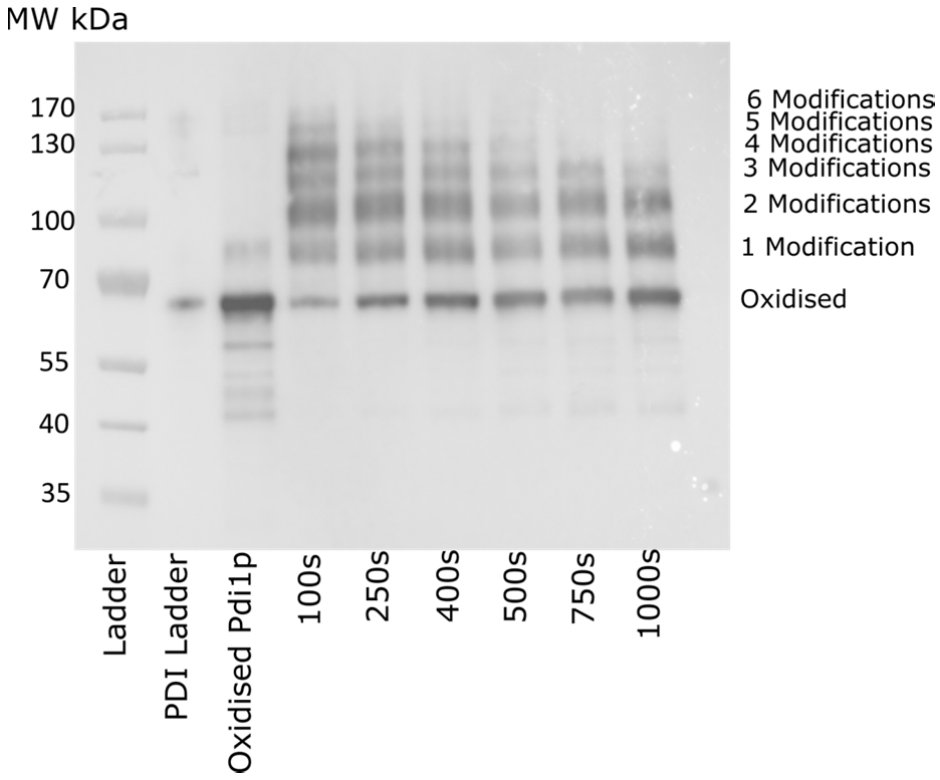

Figure S2. Full gel image of the data shown in Fig. 6A. Pdi1p oxidation state over the course of RNAse A reoxidation by Pdi1p (5 µM) and Ero1p (1 µM) was assessed by 5k PEG maleimide modification and SDS PAGE/Western blotting.

Beal et al SUPPLEMENTARY FIGURE S3

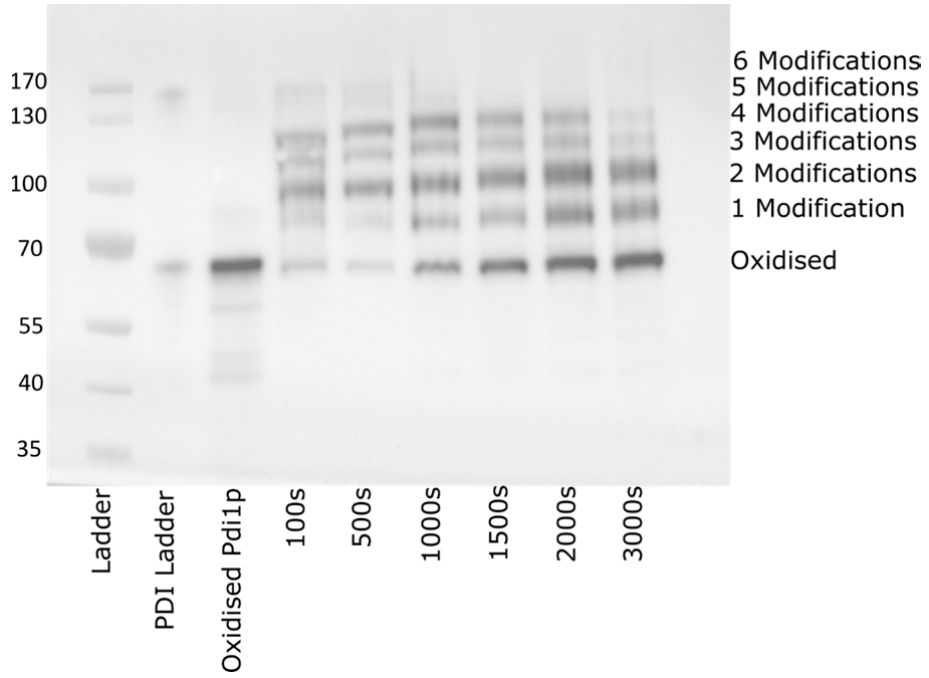

Figure S3. Full gel image of the data shown in Figure 6B. Pdi1p oxidation state over the course of RNAse A reoxidation by Pdi1p (1 µM) and Ero1p (1 µM) was assessed by 5k PEG maleimide modification and SDS PAGE/Western blotting.

Beal et al SUPPLEMENTARY FIGURE S4

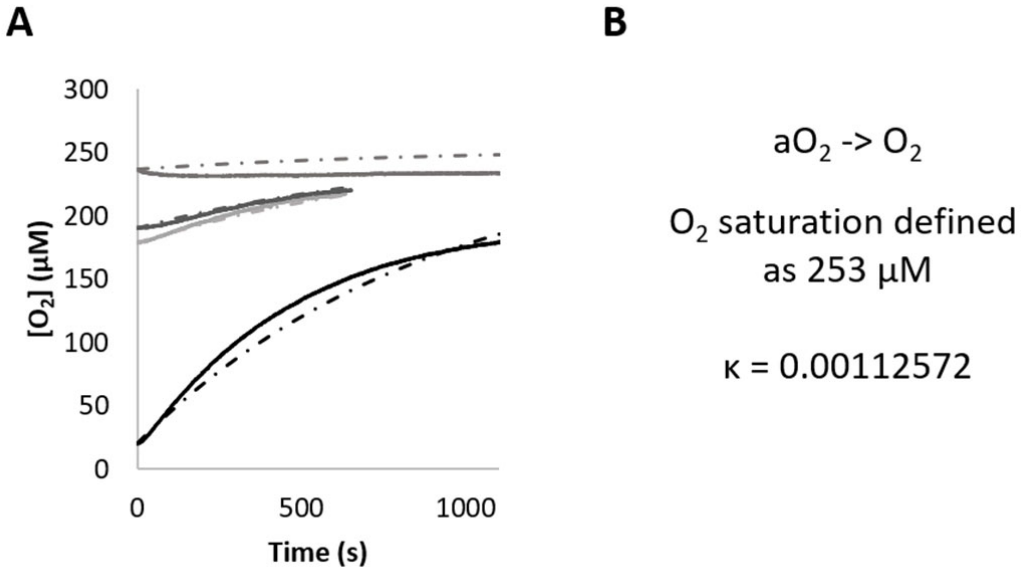

Figure S4. Determination of the rate of O_2 diffusion into the electrochemical cell during experiments. A. Solid lines: O_2 diffusion back into the electrochemical cell after sodium dithionite depletion of O_2. Dotted lines: Copasi modelled fit of O_2 diffusion into electrochemical cell. **B**. Reaction term used to define the O_2 diffusion into the electrochemical cell. aO_2 = atmospheric oxygen. The rate term, k, used in the full model.

Beal et al SUPPLEMENTARY FIGURE S5

$$\frac{\delta([H_2O_2] * V_{Compartment})}{\delta t} = +V_{Compartment} * (k1 * [yEro1r] * [O_2])$$

$$\frac{\delta([O_2] * V_{Compartment})}{\delta t} = -V_{Compartment} * (k1 * [yEro1r] * [O_2]) + V_{Compartment} * (k8 * (0.000253 - [O_2]))$$

$$\frac{\delta([yEro1o] * V_{Compartment})}{\delta t} = +V_{Compartment} * (k1 * [yEro1r] * [O_2]) - V_{Compartment} * (k2 * [yEro1o] * [yPDIr]) + V_{Compartment} * (k7 * [yEro1i] * [yPDIr])$$

$$\frac{\delta([yEro1r] * V_{Compartment})}{\delta t} = -V_{Compartment} * (k1 * [yEro1r] * [O_2]) + V_{Compartment} * (k3 * [yEro1yPDI])$$

$$\frac{\delta([yEro1yPDI] * V_{Compartment})}{\delta t} = +V_{Compartment} * (k2 * [yEro1o] * [yPDIr]) - V_{Compartment} * (k3 * [yEro1yPDI])$$

$$\frac{\delta([yPDIr] * V_{Compartment})}{\delta t} = -V_{Compartment} * (k2 * [yEro1o] * [yPDIr]) + V_{Compartment} * (k5 * [yPDIGSH] * [GSH]) - V_{Compartment} * (k6 * [yEro1i2] * [yPDIr]) - V_{Compartment} * (k7 * [yEro1i1] * [yPDIr])$$

$$\frac{\delta([yPDIo] * V_{Compartment})}{\delta t} = +V_{Compartment} * (k3 * [yEro1yPDI]) - V_{Compartment} * (k4 * [yPDIo] * [GSH]) + V_{Compartment} * (k6 * [yEro1i2] * [yPDIr]) + V_{Compartment} * (k7 * [yEro1i1] * [yPDIr])$$

$$\frac{\delta([GSH] * V_{Compartment})}{\delta t} = -V_{Compartment} * (k4 * [yPDIo] * [GSH]) - V_{Compartment} * (k5 * [yPDIGSH] * [GSH])$$

$$\frac{\delta([yPDIGSH] * V_{Compartment})}{\delta t} = +V_{Compartment} * (k4 * [yPDIo] * [GSH]) - V_{Compartment} * (k5 * [yPDIGSH] * [GSH])$$

$$\frac{\delta([GSSG] * V_{Compartment})}{\delta t} = +V_{Compartment} * (k5 * [yPDIGSH] * [GSH])$$

$$\frac{\delta([aO_2] * V_{Compartment})}{\delta t} = -V_{Compartment} * (k8 * (0.000253 - [O_2]))$$

$$\frac{\delta([yEro1i1] * V_{Compartment})}{\delta t} = +V_{Compartment} * (k6 * [yEro1i2] * [yPDIr]) - V_{Compartment} * (k7 * [yEro1i1] * [yPDIr])$$

$$\frac{\delta([yEro1i2] * V_{Compartment})}{\delta t} = -V_{Compartment} * (k6 * [yEro1i2] * [yPDIr])$$

yEro1r + O2 -> yEro1o + H2O2	**κ1**	**87500 $M^{-1}s^{-1}$**
yEro1o + yPDIr -> yEro1yPDI	**κ2**	**207234 $M^{-1}s^{-1}$**
yEro1yPDI -> yPDIo + yEro1r	**κ3**	**2.27739 s^{-1}**
yPDIo + GSH -> yPDIGSH	**κ4**	**73.9823 $M^{-1}s^{-1}$**
yPDIGSH + GSH -> yPDIr + GSSG	**κ5**	**73.9823 $M^{-1}s^{-1}$**
yEro1i2 + yPDIr -> yEro1i1 + yPDIo	**κ6**	**5327.7 $M^{-1}s^{-1}$**
yEro1i1 + yPDIr -> yEro1o + yPDIo	**κ7**	**5327.7 $M^{-1}s^{-1}$**
aO2 -> O2	**κ8**	**0.00112572 s^{-1}**

Figure S5. Differential equations describing Pdi1p and Ero1p mediated O_2 consumption produced by COPASI

Beal et al SUPPLEMENTARY FIGURE S6

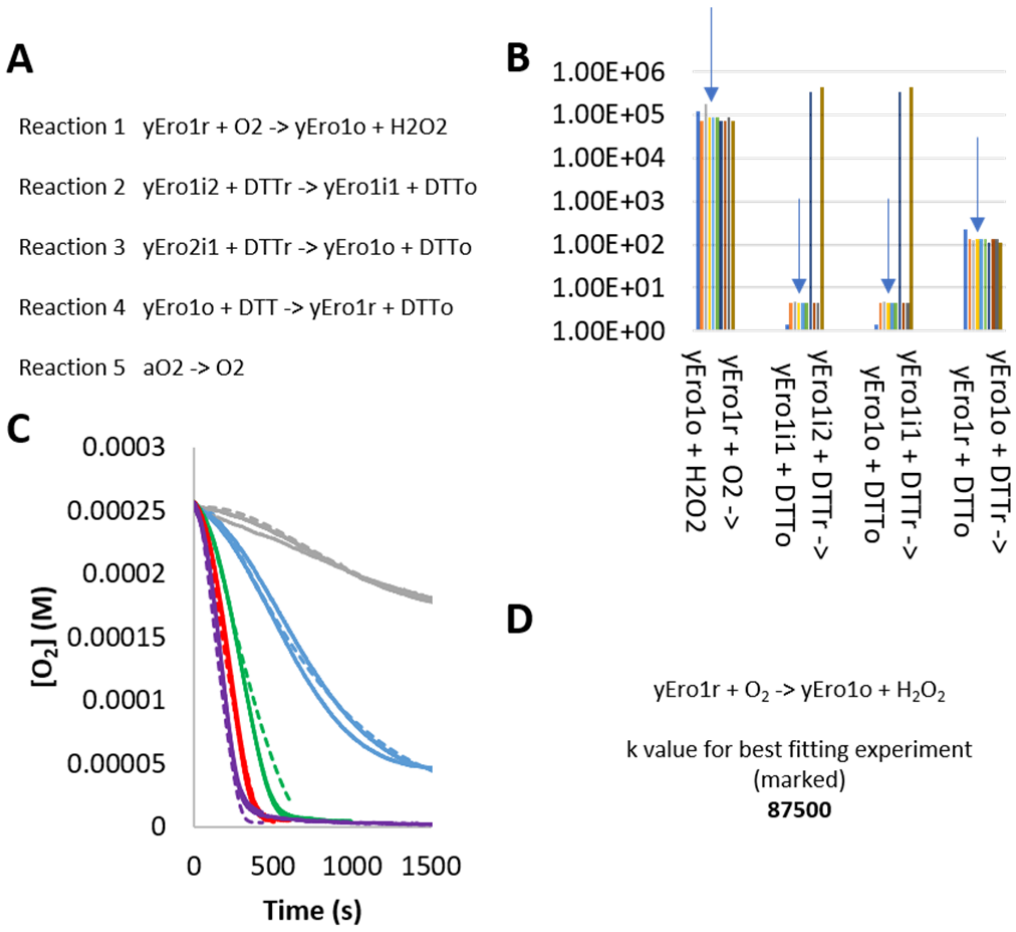

Figure S6. Determination of yEro1r oxidation rate constant from DTT reduction data. A. Reaction schemes describing yEro1 reduction by DTT and reoxidation by O_2. Making the rate of Reaction 2 and 3 the same and 4 different gives a better fit for the data but also mimics the full model (**Fig. 8A**) better. **B**. Parameter fitting of O_2 consumption data from Ero1p reduction with differing concentrations of DTT was repeated 10 times, which gave excellent reproducibility. The run, marked with an arrow, gave the best fitting data. **C**. O_2 consumption plot of experimentally derived data, solid lines, plotted against the data predicted using the rate terms determined by the best fitting run, marked with arrows on B. **D**. The rate value for the reaction common to both the DTT reaction scheme and the full model.

Beal et al SUPPLEMENTARY FIGURE S7

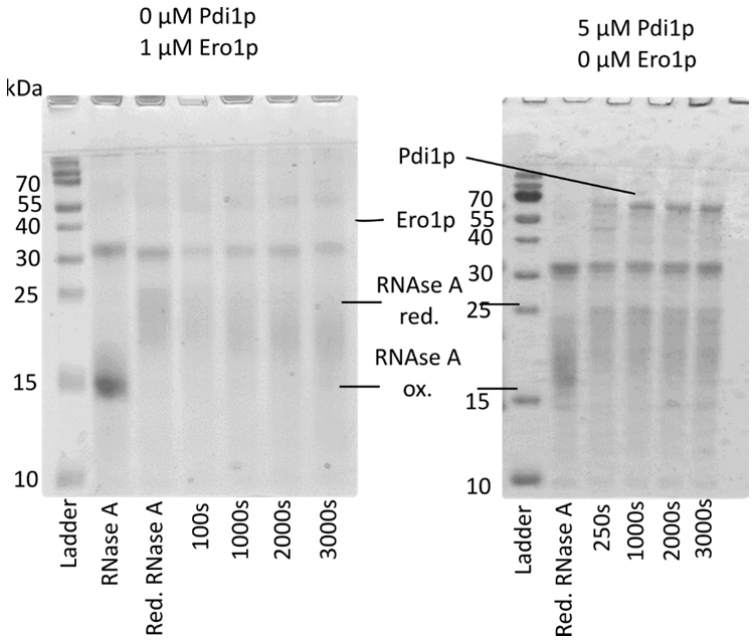

Figure S7. SDS PAGE analysis of the oxidation of RNAse A in absence Pdi1p and Ero1p. The oxidation state of RNAse A was assessed, by AMS trapping, over a similar duration to the experiments of x and S1, where either Pdi1p (left) or Ero1p (right) were not added to the reaction. Left – 0 µM Pdi1p, 1 µM Ero1p and 60 µM rRNAse A. Right - 5 µM Pdi1p, 0 µM Ero1p and 60 µM rRNAse. This data shows that in the absence of either component the amount during the timeframe of the experiment the degree of spontaneous RNAse A oxidation was minimal.

Beal et al SUPPLEMENTARY FIGURE S9

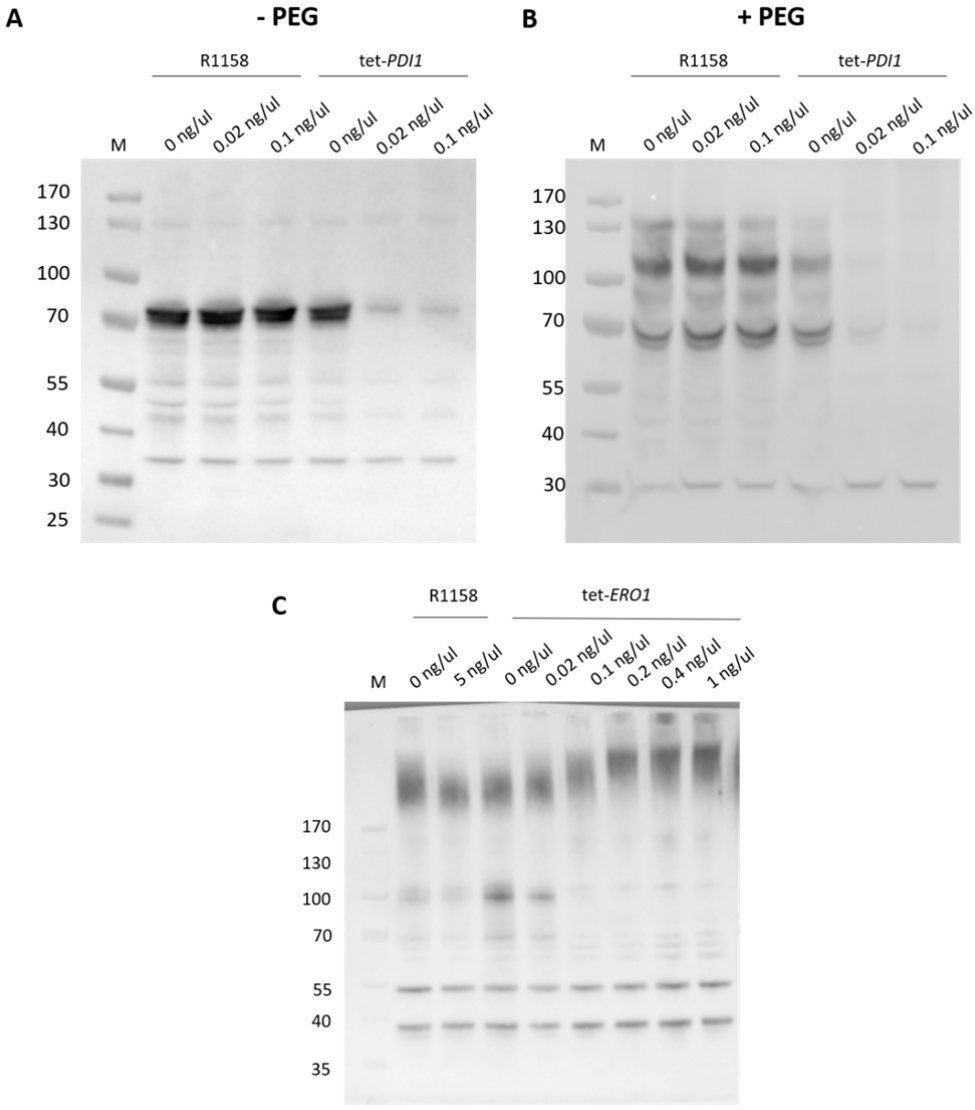

Figure S9. Full gel image of the data shown in Figure 8. This figure presents analyses of strains where expression of the *PDI1* or *ERO1* genes was place under control of a doxycycline-repressible promoter (Tet-Pdi1 and Tet-Ero1, respectively), compared to isogenic control strains containing the natural promoters (R1158). **A -** shows levels of Pdi1p in the tet-*PDI1* strain without PEG maleimide trapping. B **-** Shows the redox state of Pdi1p by PEG maleimide trapping of the tet-*PDI1* strain. **C –** Shows the levels of Ero1p in the tet-*ERO1* strain.